Responses to Reviewer #1

General Comments: This is a well written and, in general, clearly presented paper that seems to present a good case for the dominance of nitrates for aerosols concentrations in the upper troposphere and lower stratosphere over the Asian summer monsoon sector. I have made suggestions for minor revisions.

My primary criticism concerns the comparisons of observed and modeled concentrations of O_3 and HNO_3. The authors claim that observed concentrations are well represented by the model, but offer no context for that comparison. I think the authors should answer the question: Given the discrepancies between observed and modeled O_3 and HNO_3 – what are the uncertainties of modeled nitrate concentrations?

Sec. 4.2 and Fig. 8, which compares modeled concentrations to in situ surface observations, should be deleted. While it is interesting to see such comparisons, the sampling is poor, which, together with the mismatch of sampling time, makes the comparisons difficult to interpret.

Sec. 4.3 shows the comparison of vertical distributions of aerosol extinction from the model with SAGE observations. Comparisons of horizontal distributions in the UTLS should be performed as well.

Responses to general comments:

We have addressed the major issues mentioned in the general comments:

(1) We now give quantitative descriptions on the discrepancies between observed and simulated O_3 and HNO_3. We have added the following sentences for HNO_3 in the third paragraph of Section 3.1: "At 100 hPa, the observed HNO_3 mixing ratio averaged over the TP/SASM region (70–105°E, 10–40°N) is 301.3 pptv, which is lower than the simulated value of 349.1 pptv. The difference between the simulated and observed HNO_3 mixing ratio lies within the confidence range of ±500–1000 pptv of the MLS instruments (Livesey et al., 2011). Considering all the grid cells with MLS HNO_3 data available, the simulated seasonal mean HNO_3 concentrations show normalized mean bias (NMB) of +15.9% at 100 hPa over the TP/SASM region (70–105°E, 10–40°N) in summer of year 2005." We have added the following sentences for O_3 in the second paragraph of Section 3.2: "At 100 hPa, simulated and MLS observed O_3 mixing ratios averaged over the TP/SASM region (70–105°E, 10–40°N) are 190.6 and 145.1 ppbv, respectively. Compared to MLS observations, simulated O_3 concentrations at 100 hPa have a NMB of +31.4% over the TP/SASM region in summer of 2005." We have also

added a sentence in the second paragraph of the conclusion section: "At 100 hPa, simulated seasonal mean HNO_3 and O_3 mixing ratios show NMBs of +15.9% and +31.4%, respectively, over the TP/SASM region (70−105°E, 10−40°N) in summer of year 2005."

(2) We have performed several new sensitivity studies to examine the uncertainties with simulated nitrate concentrations in the UTLS. Anthropogenic emissions of NO_x, NH_3, and SO_2 are changed according to the NMBs of the simulated concentrations of sulfate and nitrate. These sensitivity studies all confirm that nitrate aerosol is a dominant aerosol species in the UTLS, which are presented in our new Section 7 of "Impacts of uncertainties in surface-layer aerosol concentrations on simulated nitrate in the UTLS".

(3) The comparisons of simulated surface-layer aerosol concentrations with observations in Section 4.2 are performed to evaluate the model's ability to simulate various aerosols. Considering yours and the other reviewer's suggestions on discussions of uncertainties associated with simulated nitrate in the UTLS, we have performed several sensitivity studies on the basis of the biases in simulated surface-layer aerosols (see our new Section 7). Thus, we prefer to retain Section 4.2 and Fig. 8 in the revised manuscript.

(4) It is difficult to compare the simulated horizontal distributions of aerosol extinction coefficient with SAGE II observations, because SAGE II data do not provide the information on horizontal distribution for a specific month. The SAGE II instrument vertically scans the limb of the atmosphere during spacecraft sunsets and sunrises (fifteen sunsets and fifteen sunrises each day). The 57 degrees inclined orbit of the ERBS spacecraft evenly distributes the SAGE II measurements every 24 degrees of longitude along a slowly shifting latitude circle. (http://www.nasa.gov/centers/langley/news/factsheets/SAGE.html). For the anticyclone region of (20–120°E, 10–40°N), the measurements are available at about 28 sites and each site has only one profile during the month of July in 2005. Therefore, we average the profiles observed over the region of our interest during the month of July in 2005 to compare monthly vertical distribution of aerosol extinction in our manuscript.

Our point-to-point responses to the reviewer's comments are listed below.

Specific Comments:

1. Page 32050, Lines 9-10: Mention that $PM_{2.5}$ is the sum of the previous aerosols listed.
Response:
    We have clarified here that $PM_{2.5}$ is the sum of sulfate, nitrate, ammonium, black carbon, and organic carbon aerosols.

2. Page 32050, Line 12: It would be better to state that nitrate is of secondary importance near the surface. There are other aerosols that have as large (or

nearly as large) concentrations; stating that nitrate has the second largest concentration without acknowledging that other aerosols are as important is not a fair assessment.

Response:

We have revised the sentence as "Nitrate aerosol is simulated to be of secondary importance near the surface but the most dominant aerosol species in the UTLS over the studied region."

3. p. 32050, l. 22: Change 'time to 'times'

Response:

Changed.

4. p. 32050, l. 22: Change 'which influence' to 'influencing'

Response:

Changed.

5. p. 32051, l. 16,17: Remove 'M.' from 'M. Park'

Response:

Because there are two references of Park et al. (2004) in the manuscript, 'M.' was added to one of them by the journal's Production Office.

6. p. 32053, l. 1: Remove '(> 75%)'

Response:

Removed.

7. p. 32056, l. 17-18: Seasonal cycles if SO_2, OC and BC are very weak.

Response:

Yes, the seasonal cycles of SO_2, OC, and BC are week. We have deleted the sentence of "Emissions of SO_2, OC and BC are the highest during wintertime as a result of the winter heating."

8. p. 32057, Fig. 3a: Why are concentrations high (the highest of any region) over south equatorial Africa?

Response:

As discussed in Liao et al. (2003), high concentrations of HNO_3 over south equatorial Africa result from high biomass burning emissions in that region in summer of every year. We have clarified in the text that "Concentrations of HNO_3 exceed 1 ppbv over the industrialized areas such as Europe, North America, central and eastern Asia, and over biomass burning regions in the tropics, in agreement with the distributions and magnitudes reported in Liao et al. (2003)."

9. p. 32058, Fig. 4: There are factor of 2 (and greater) discrepancies between model and observations – how does this uncertainty translate into an

uncertainty in nitrate aerosol?

Response:

We have added in the third paragraph of Section 3.1 the quantitative description on the discrepancies between observed and simulated HNO_3: "Considering all the grid cells with MLS HNO_3 data available, the simulated seasonal mean HNO_3 concentrations show normalized mean bias (NMB) of +15.9% at 100 hPa over the TP/SASM region in summer of year 2005."

The uncertainties in HNO_3 and nitrate are associated with the uncertainties in anthropogenic emissions of chemical species such as NO_x, NH_3, and SO_2. We have performed several sensitivity studies to examine the uncertainties of simulated nitrate concentrations, as we present in our new Section 7 "Impacts of uncertainties in surface-layer aerosol concentrations on simulated nitrate in the UTLS".

10. p. 32060, l. 25: Concentrations of ammonium and organic carbon are just as (or nearly as) large as nitrate – though technically accurate, it is misleading to state that nitrate is the second largest without acknowledging that other aerosols are just as important.

Response:

We have revised the description as "NO_3^- is simulated to be of secondary importance at the surface over the region of our interest."

11. p. 32062, l. 8: Change '8b-j' to '8b-f'

Response:

Changed.

12. p. 32064, Table 2: Certain values in Table 2 do not make sense and indicate that the calculations of concentration are not performed consistently among constituents. This is most obvious for values of concentrations averaged over TP/SASM that are smaller than the corresponding values for the individual TP and SASM. If the concentrations are calculated in a consistent manner then the values for TP/SASM have to lie between the values for TP and those for SASM. Please check these the accuracy of the calculations or, if the calculations are not consistent by design, please explain why.

Response:

Thanks for pointing this out. We have recalculated the concentrations in a consistent manner and the new results are displayed in Table 2.

13. p. 32065, l. 16-17: Explain why you are not using winds used in GEOS-CHEM.

Response:

The assimilated GEOS-5 meteorological fields used to drive the GEOS-Chem simulation do not have vertical winds

(http://wiki.seas.harvard.edu/geos-chem/index.php/List_of_GEOS-5_met_field s), so we use the ECMWF reanalysis wind fields to do the analysis. This is now explained in the text.

14. p. 32066, Sec. 6.2: Explain why you are not able to use GEOS-CHEM chemistry to determine precisely what the mechanisms for nitrate formation are.
Response:
   The chemical mechanism for nitrate formation in the GEOS-Chem model was described in R. J. Park et al. (2004), which is comprehensive and has been used extensively in previous studies to simulate nitrate aerosol (R. J. Park et al., 2004; Pye et al., 2009; Zhang et al., 2010; Zhu et al., 2012; Jiang et al., 2013; Lou et al., 2014). The same chemistry mechanism was also used to examine the global distributions and concentrations of nitrate aerosol in Liao et al. (2004) and Liao and Seinfeld (2005). Nitrate forms from the partitioning of HNO_3 between gas and aerosol phases. Major reactions for the production and loss of HNO_3 were listed in Liao and Seinfeld (2005) (see Table R1 below). Therefore the formation of gas-phase HNO_3 and the partitioning of HNO_3 between gas and aerosol phases are the two major chemical processes that influence nitrate concentrations. We have evaluated the ability of the GEOS-Chem model to simulate gas-phase HNO_3 in Section 3.1 (by comparisons of our model results with MLS observations and concentrations from previous modeling studies), so we quantify in Section 6.2 the nitrate formation from gas-to aerosol conversion of HNO_3 based on the ISORROPIA II thermodynamic equilibrium module (Fountoukis and Nenes, 2007) in the GEOS-Chem model. We have added these explanations in Sections 6.1 and 6.2.

Table R1. Annual mean HNO_3 budget for present-day and year 2100 simulations (taken from Liao and Seinfeld, 2005)

	Present-Day		Year 2100	
	Baseline	NOHET	Baseline	NOHET
Chemical Productions, Tg yr^{-1}	153.5	154.5	464.0	457.3
(R1) $NO_2 + OH + M \rightarrow HNO_3 + M$	36.5%	55.5%	36.8%	61.8%
(R2) $NO_3 + CH_2O \rightarrow HNO_3 + prod.$	1.1%	3.8%	2.2%	8.9%
(R3) $ALD2 + NO_3 \rightarrow HNO_3 + prod.$	0.8%	3.2%	1.8%	6.6%
(R4) $RIO2 + NO \rightarrow HNO_3 + prod.$	9.3%	9.1%	3.9%	3.7%
(R5) $RIO1 + NO \rightarrow HNO_3 + prod.$	0.8%	0.7%	0.4%	0.3%
(R6) $IAO2 + NO \rightarrow 0.08HNO_3 + prod.$	0.3%	0.3%	0.1%	0.1%
(R7) $VRO2 + NO \rightarrow HNO_3 + prod.$	0.9%	0.9%	0.4%	0.4%
(R8) $MRO2 + NO \rightarrow HNO_3 + prod.$	0.6%	0.6%	0.3%	0.2%
(R9) $MVN2 + NO \rightarrow 0.1HNO_3 + prod.$	0.0%	0.1%	0.0%	0.1%
(R10) $INO2 + NO \rightarrow 0.85HNO_3 + prod.$	4.7%	5.8%	2.6%	3.6%
(R11) $ALK4 + NO_3 \rightarrow HNO_3 + prod.$	0.0%	0.4%	0.1%	0.5%
(R12) $RCHO + NO_3 \rightarrow HNO_3 + prod.$	0.1%	0.4%	0.2%	0.7%
(R13) $MEK + NO_3 \rightarrow HNO_3 + prod.$	1.1%	3.3%	0.8%	2.9%
(R14) $INO2 + MO2 \rightarrow 0.425HNO_3 + prod.$	0.6%	0.8%	0.2%	0.3%
(R15) $GLYX + NO_3 \rightarrow HNO_3 + prod.$	0.0%	0.0%	0.0%	0.0%
(R16) $MGLY + NO_3 \rightarrow HNO_3 + prod.$	0.2%	0.8%	0.3%	1.5%
(R17) $MACR + NO_3 \rightarrow HNO_3 + prod.$	0.3%	0.7%	0.2%	0.8%
(R18) $C_2H_6 + NO_3 \rightarrow HNO_3 + prod.$	0.0%	0.0%	0.1%	0.2%
(R19) $INO2 + MCO3 \rightarrow 0.85HNO_3 + prod.$	2.2%	2.8%	1.0%	1.1%
(R20) $DMS + NO_3 \rightarrow HNO_3 + prod.$	7.4%	10.8%	4.1%	6.3%
(R21) $NO_2 + (aerosols) \rightarrow 0.5HNO_3 + prod.$	6.2%	0.0%	8.2%	0.0%
(R22) $NO_3 + (aerosols) \rightarrow HNO_3 + prod.$	0.3%	0.0%	0.4%	0.0%
(R23) $N_2O_5 + (aerosols) \rightarrow 2HNO_3$	26.5%	0.0%	35.8%	0.0%
Total loss, Tg yr^{-1}	153.5	154.5	464.0	457.3
Chem. loss, Tg yr^{-1}	10.7	20.0	24.9	44.6
(R24) $HNO_3 + OH \rightarrow prod.$	34.6%	37.0%	32.9%	36.8%
(R25) $HNO_3 + hv \rightarrow prod.$	65.4%	63.0%	67.1%	63.2%
Dust uptake, Tg yr^{-1}	37.1	0	73.0	0
Loss to nitrate,^{b} Tg yr^{-1}	36.9 (105.3−68.4)	46.0 (123.5−77.5)	168.7 (394.4−225.7)	176.1 (470.7−294.6)
Dry deposition, Tg yr^{-1}	27.3	35.6	80.1	97.2
Wet deposition, Tg yr^{-1}	41.5	52.9	117.3	139.4
Burden, Tg	1.30	1.78	2.16	2.98

^{a}The numbers for reactions (R1)−(R25) are contributions to chemical production or loss from each reaction. Please see http://www.as.harvard.edu/chemistry/trop/geos/doc/chem_mech/geoschem_mech.pdf for the formula of the species in these reactions and for the rate constants.
^{b}The first number in the parentheses is the loss of gas-phase HNO_3 to nitrate formation, and the second number shows the release of gas-phase HNO_3 from nitrate, which are determined by aerosol thermodynamics.

15. p. 32066, l. 17: Change 'in consistent' to 'consistent'.
Response:
    Changed.

16. p. 32066, l. 21-22: Delete the sentence 'Besides being . . .'. It is not clear that cold temperatures near the tropopause have a casual influence on upwelling there nor is it important to your study for that to be the case.
Response:
    Deleted as suggested.

17. p. 32067, l. 19: Change 'scarcely' to 'are not' or change 'particles in the UTLS of the TP/SASM scarcely composed of coarse and aspherical particles such as NAT' to 'coarse and aspherical particles such as NAT are scarce in the UTLS of the TP/SASM'.
Response:
    Thanks for the suggestion. We have changed "particles in the UTLS of the TP/SASM scarcely composed of coarse and aspherical particles such as NAT" to "coarse and aspherical particles such as NAT are scarce in the UTLS of the TP/SASM".

18. p. 32067, l. 23: Delete 'by simulation'.
Response:
    Deleted.

19. p. 32067, l. 26: Change 'capability in simulating' to 'ability to simulate'.

Response:
    Changed.

20. p. 32068, l. 1: Regarding 'agree well'. You need to put the model-observations comparisons into the context of nitrate formation in order to say they agree well. That is, you need to determine what the uncertainties of nitrate concentrations are given the uncertainties of O_3 and HNO_3 concentrations (as determined by the model-observation discrepancies).
Response:
    We now give quantitative descriptions on the discrepancies between observed and simulated O_3 and HNO_3: "At 100 hPa, simulated seasonal mean HNO_3 and O_3 mixing ratios show NMBs of +15.9% and +31.4%, respectively, over the TP/SASM region (70−105°E, 10−40°N) in summer of year 2005". The discussions on uncertainties in simulated nitrate concentrations are presented in our new Section 7.

21. p. 32068, l. 8: Regarding 'second largest'. See above comment for p. 32060, l. 25.
Response:
    We have revised the description as "Nitrate aerosol is simulated to be of secondary importance near the surface over the region of our interest."

22. p. 32068, l. 17: Instead of 'the GEOS-CHEM model reproduces well', state how well it reproduces (e.g., with 10% or whatever) observed values.
Response:
    We have added one quantitative sentence here: "The discrepancies between the simulated and observed aerosol extinction coefficient are within 8% in the UTLS (averaged over 14−16 km)."

23. p. 32068, l. 29: Change 'convections' to 'convection'.
Response:
    Changed.

References:
Fountoukis, C., and Nenes, A.: ISORROPIA II: a computationally efficient thermodynamic equilibrium model for $K^+–Ca^{2+}–Mg^{2+}–NH_4^+–Na^+–SO_4^{2-}–NO_3^-–Cl^-–H_2O$ aerosols, Atmos. Chem. Phys., 7, 4639–4659, 2007.
Jiang, H., Liao, H., Pye, H., Wu, S., Mickley, L. J., Seinfeld, J. H., and Zhang, X.: Projected effect of 2000–2050 changes in climate and emissions on aerosol levels in China and associated transboundary transport, Atmos. Chem. Phys., 13, 7937–7960, 2013.

Liao, H., Adams, P. J., Chung, S. H., Seinfeld, J. H., Mickley, L. J., and Jacob, D. J.: Interactions between tropospheric chemistry and aerosols in a unified general circulation model, J. Geophys. Res., 108, 4001, doi:10.1029/2001JD001260, 2003.

Liao, H., Seinfeld, J. H., Adams, P. J., and Mickley L. J.: Global radiative forcing of coupled tropospheric ozone and aerosols in a unified general circulation model, J. Geophys. Res., 109, D16207, doi:10.1029/2003JD004456, 2004.

Liao, H., and Seinfeld, J. H.: Global impacts of gas-phase chemistry-aerosol interactions on direct radiative forcing by anthropogenic aerosols and ozone, J. Geophys. Res., 110, D18208, doi:10.1029/2005JD005907, 2005.

Livesey, N. J., Read, W. G., Wagner, P. A., Froidevaux, L., Lambert, A., Manney, G. L., Pumphrey, H. C., Santee, M. L., Schwartz, M. J., Wang, S., Cofield, R. E., Cuddy, D. T., Fuller, R. A., Jarnot, R. F., Jiang, J. H., and Knosp, B. W.: Version 3.3 Level 2 data quality and description document, JPL D-33509, 2011.

Lou, S., Liao, H., and Zhu, B.: Impacts of aerosols on surface-layer ozone concentrations in China through heterogeneous reactions and changes in photolysis rates, Atmos. Environ., 85, 123-138, doi:10.1016/j.atmosenv.2013.12.004, 2014.

Park, M., Randel, W. J., Kinnison, D. E., Garcia, R. R., and Choi, W.: Seasonal variation of methane, water vapor, and nitrogen oxides near the tropopause: Satellite observations and model simulations, J. Geophys. Res., 109, D03302, doi:10.1029/2003JD003706, 2004.

Park, R. J., Jacob, D. J., Field, B. D., Yantosca, R. M., and Chin, M.: Natural and transboundary pollution influences on sulfate-nitrate-ammonium aerosols in the United States: Implications for policy, J. Geophys. Res., 109, D15204, doi:10.1029/2003JD004473, 2004.

Pye, H., Liao, H., Wu, S., Mickley, L. J., Jacob, D. J., Henze, D. K., and Seinfeld, J.: Effect of changes in climate and emissions on future sulfate–nitrate–ammonium aerosol levels in the United States, J. Geophys. Res., 114, D01205, doi:10.1029/2008JD010701, 2009.

Zhang, L., Liao, H., and Li, J.: Impacts of Asian summer monsoon on seasonal and interannual variations of aerosols over eastern China, J. Geophys. Res., 115, D00K05, doi:10.1029/2009JD012299, 2010.

Zhu, J., Liao, H., and Li, J.: Increases in aerosol concentrations over eastern China due to the decadal-scale weakening of the East Asian summer monsoon, Geophys. Res. Lett., 39, L09809, doi:10.1029/2012GL051428, 2012.

Responses to Reviewer #2

General Comments: This study investigates the spatial distribution of nitrate aerosols in the UTLS over the Tibetan Plateau and the South Asian summer monsoon (TP/SASM) region using the GEOS-Chem model. With GEOS-Chem, the authors simulate elevated concentrations of summertime aerosols in the UTLS over the TP/SASM region, confirming the findings of previous observation and model studies. In contrast to previous model studies, which generally emphases the importance of sulfate, they argue that nitrate aerosol is the most dominant aerosol species in the UTLS over the studied region. According to their model result, nitrate contributes more than half of the aerosol mass concentration ($PM_{2.5}$) at 100 hPa height. The issue addressed by this study is interesting and is within the scope of ACP. The manuscript is well written and organized, but the scientific quality of the current manuscript is not sufficiently high for publication. The authors may consider performing additional model analyses to provide stronger evidence to support their arguments.

Responses to general comments:

We have performed additional sensitivity studies to examine the uncertainties associated with simulated nitrate in the UTLS. Anthropogenic emissions of NO_x, NH_3, and SO_2 are changed according to the NMBs of the simulated concentrations of sulfate and nitrate. These sensitivity studies all confirm that nitrate aerosol is a dominant aerosol species in the UTLS, which are presented in our new Section 7 of "Impacts of uncertainties in surface-layer aerosol concentrations on simulated nitrate in the UTLS".

Our point-to-point responses to the reviewer's comments are listed below.

Specific Comments:

1. The study is focused on aerosol formation in the UTLS, a region influenced by both tropospheric and stratospheric processes. In contrast to complete tropospheric chemistry, the simplification of stratospheric chemistry in GEOS-Chem and possible influence on HNO_3 and nitrate aerosol formation in the UTLS is not well introduced in the manuscript. It is stated that the chemical reaction rates in the stratosphere are taken from other model than GEOS-Chem (Line 190-195). The authors performed a 10-year spin-up run to generate the initial conditions (Line 239-241). How are the long-lived species like CFCs and N_2O are treated in the model? Could the year 2005 stratospheric chemistry be simulated?

Response:

(1) Both CFCs and N_2O are considered in the linearized stratospheric chemistry in the GEOS-Chem model, and their concentrations are updated at the end of each chemistry time step by using the archived three-dimensional monthly mean production rates and loss frequencies from the NASA Global

Modeling Initiative (GMI) Combo simulations. More details are described at http://wiki.seas.harvard.edu/geos-chem/index.php/Stratospheric_chemistry and in Murray et al. (2012).

We have revised the description on stratospheric chemistry in Section 2.1:" The monthly mean production rates and loss frequencies of other stratospheric species (including long-lived species such as CFCs and N_2O) use those from NASA Global Modeling Initiative (GMI) Combo simulations (Duncan et al., 2007; Considine et al., 2008; Murray et al., 2012)."

(2) The archived three-dimensional monthly mean production rates and loss frequencies in the stratosphere are the averages over years of 2004–2010 (http://wiki.seas.harvard.edu/geos-chem/index.php/Stratospheric_chemistry). Although we use the emissions and meteorological fields of year 2005 in our simulations, we would consider that the tropospheric simulation can be representative of year 2005 but stratosphere simulation should represent a multi-year average. This is now clarified in Section 2.2 where we describe our numerical experiments.

2. HNO_3 concentrations from MLS are used for comparison with model results in this study. As shown in Fig. 4, however, no MLS data are available at 200 hPa and 100 hPa over most of the TP/SASM region. Surface concentrations of aerosols in the SASM region are also used for model evaluation, with normalized mean biases of +51.5% for NO_3^- and 74.9% for NH_4^+ in summertime. What are the causes of such large biases? Do such large biases have great impact on the simulation of nitrate in the UTLS, as upward transport from the lower troposphere is suggested to be a mechanism for high nitrate concentrations in the UTLS? Specifically, might the concentrations of nitrate aerosol in the UTLS be greatly overestimated as well?
Response:

(1) Since dense high clouds were observed to locate in the upper troposphere over the Tibetan Plateau (Li et al., 2005), most cloud-contaminated measurements were screened out for MLS v4.2 datasets as described in Lively et al. (2015). As a result, no MLS data are available at 200 hPa and 100 hPa over a large fraction of the TP/SASM region. To have more datasets for comparisons between the simulations and the observations, we have replaced MLS 4.2 datasets with MLS v3.3 datasets, which have been widely used in previous studies (Livesey et al., 2011; Miyazaki et al., 2012; Fiorucci et al., 2013; Schwartz et al., 2015; Yan et al., 2015). The MLS v3.3 measurements are available in about 60% of the grid cells at 200 hPa and in about 95% of the grid cells at 100 hPa over the TP/SASM region (70–105°E, 10–40°N). We have added the following sentence for HNO_3 in the third paragraph of Section 3.1: "Considering all the grid cells with MLS HNO_3 data available, the simulated seasonal mean HNO_3 concentrations show normalized mean bias (NMB) of +15.9% at 100 hPa over the TP/SASM region in summer of year 2005."

(2) As noted in Section 4.2 of the manuscript, the reasons for the large NMBs of NO_3^- and NH_4^+ include (a) the measurements of NO_3^- and NH_4^+ are quite limited in terms of the number of samples, and (b) the mismatch of the model year 2005 with the years of 1992–2010 with observations available.

(3) We have performed four new sensitivity studies to examine the impacts of uncertainties in surface-layer aerosol concentrations on simulated nitrate in the UTLS. In the first three cases, anthropogenic emissions of NO_x, NH_3, and SO_2 in Asia are changed by −50%, −50%, and +20%, respectively, relative to those in our standard simulation. In the last case, anthropogenic emissions of all these three species are changed simultaneously, with NO_x reduced by 50%, NH_3 reduced by 50%, and SO_2 increased by 20% in Asia relative to the standard simulation. All these sensitivity studies confirm that nitrate is the most dominant aerosol species in summertime in the UTLS over the TP/SASM region (see Table 3 below). See also our new Section 7 "Impacts of uncertainties in surface-layer aerosol concentrations on simulated nitrate in the UTLS" in the revised manuscript.

Table 3. Sensitivity simulations to examine the impacts of uncertainties in surface-layer aerosol concentrations on simulated NO_3^- in the UTLS. "Conc" and "Ctri" denote, respectively, simulated seasonal mean concentrations of SO_4^{2-}, NO_3^-, NH_4^+, OC, BC and their contributions to PM$_{2.5}$ (in percentages) during summertime (June-August) of 2005. The mass concentrations are averaged over the TP/SASM region, with unit of $\mu g\ m^{-3}$ at the surface layer and of $10^{-2}\ \mu g\ m^{-3}$ at 200 hPa and 100 hPa. Also shown are the NMBs, as the simulated surface-layer concentrations are compared with measurements described in Section 4.2.

Species	Baseline Case			SO$_2$ (+20%)			NO$_x$ (−50%)			NH$_3$ (−50%)			All Change		
	Conc.	Ctri.	NMB	Conc.	Ctri.	NMB	Conc.	Ctri.	NMB	Conc.	Ctri.	NMB	Conc.	Ctri.	NMB
Surface															
SO_4^{2-}	1.70	35.9%	−14.7%	1.92	38.1%	−4.4%	1.58	39.5%	−18.1%	1.70	38.1%	−14.7%	1.78	43.2%	−8.3%
NO_3^-	0.94	19.8%	+51.5%	0.94	18.7%	+53.5%	0.50	12.5%	−11.7%	0.73	16.4%	+24.1%	0.39	9.5%	−27.0%
NH_4^+	0.85	18.1%	+74.9%	0.94	18.6%	+93.8%	0.68	17.1%	+44.1%	0.78	17.6%	+64.6%	0.71	17.3%	+55.4%
OC	0.94	19.8%	−57.2%	0.94	18.6%	−57.2%	0.94	23.4%	−57.2%	0.94	21.0%	−57.2%	0.94	22.7%	−57.2%
BC	0.30	6.4%	−32.2%	0.30	6.0%	−32.2%	0.30	7.5%	−32.2%	0.30	6.8%	−32.2%	0.30	7.3%	−32.2%
200 hPa															
SO_4^{2-}	3.27	20.2%		3.67	22.9%		3.31	20.6%		3.29	29.1%		3.74	33.7%	
NO_3^-	7.57	46.8%		7.05	43.9%		7.41	46.0%		3.86	34.2%		3.19	28.7%	
NH_4^+	2.67	16.5%		2.67	16.6%		2.71	16.8%		1.49	13.2%		1.50	13.5%	
OC	2.22	13.7%		2.22	13.8%		2.22	13.8%		2.22	19.7%		2.22	20.0%	
BC	0.44	2.7%		0.44	2.7%		0.44	2.7%		0.44	3.9%		0.44	4.0%	
100 hPa															
SO_4^{2-}	2.60	21.4%		2.80	23.0%		2.66	21.9%		2.60	25.2%		2.87	27.2%	
NO_3^-	6.90	56.8%		6.72	55.3%		6.81	56.1%		5.68	55.0%		5.62	53.3%	
NH_4^+	1.43	11.8%		1.43	11.7%		1.45	12.0%		0.84	8.1%		0.84	8.0%	
OC	1.05	8.6%		1.05	8.6%		1.05	8.7%		1.05	10.2%		1.05	10.0%	
BC	0.16	1.3%		0.16	1.3%		0.16	1.3%		0.16	1.6%		0.16	1.5%	

3. The investigation appears to be skin-deep without in-depth analysis of physical-chemical processes. For instance, what are the different chemical mechanisms for NO3- and SO42- formation that contribute to the differences in their vertical distributions (Line 509-513)? The possibility of the nitric acid trihydrate (NAT) formation in the investigated region is discussed in this study (Line 555-566). However, while only the range of temperatures is referred, other chemical and physical conditions that are also important for the NAT formation (see Kirner et al., 2011) are not addressed. Could GEOS-Chem be used for the simulation of NAT?

Response:

(1) We have added in Section 6.1 the following detailed description on the chemical mechanisms for SO_4^{2-} and NO_3^- that contribute to the differences in their vertical distributions: "The chemical mechanisms for the formation of SO_4^{2-}, NO_3^-, and NH_4^+ aerosols in the GEOS-Chem model were described in R. J. Park et al. (2004), which are comprehensive and have been used extensively in previous studies to simulate these three aerosol species (R. J. Park et al., 2004; Pye et al., 2009; L. Zhang et al., 2010; Zhu et al., 2012; Jiang et al., 2013; Lou et al., 2014). Sulfate aerosol forms from gas-phase oxidation of SO_2 by OH and from in-cloud oxidation of SO_2 by O_3 and H_2O_2. Nitrate forms from the partitioning of HNO_3 between gas and aerosol phases, which is calculated by the ISORROPIA II thermodynamic equilibrium module (Fountoukis and Nenes, 2007) in the GEOS-Chem model. Major reactions for the production and loss of HNO_3 were listed in Liao and Seinfeld (2005). HNO_3 is produced by the reaction of NO with OH during daytime and by hydrolysis of N_2O_5 on aerosol surfaces at night. The chemical mechanisms for SO_4^{2-} and NO_3^- have different sensitivity to meteorological conditions. During the vertical transport, temperature decreases, which reduces the gas-phase oxidation of SO_2 (Yao et al., 2002; Seinfeld and Pandis 2006; X. Y. Zhang et al., 2012) but promotes the formation of NO_3^- by shifting gas-particle equilibria (Dawson et al., 2007; Liao et al., 2009). Therefore the different chemical mechanisms for SO_4^{2-} and NO_3^- formation contribute to the differences in their vertical distributions."

(2) We have revised the description on the mechanism of NAT formation, in Section 6.2: "Previous studies have also reported that nitric acid trihydrates (NAT, $HNO_3•(H_2O)_3$) could form in the polar and tropical stratosphere at low temperatures through two mechanisms: (1) the homogeneous nucleation out of supercooled ternary solutions, and (2) the heterogeneous formation on ice particles (Hofmann et al., 1989; Carslaw et al., 1998; Voigt et al., 2000; Popp et al., 2006; Kirner et al., 2011). A typical NAT condensation temperature is approximate 193 K (Kirner et al., 2011)."

Currently the GEOS-Chem model does not have simulation of NAT. The balloon-borne measurements of depolarization ratio and backscattering ratio of aerosols at Lhasa during August-October of 1999 by Kim et al. (2003) and Tobo et al. (2007) suggested that coarse and aspherical particles such as NAT are scarce in the UTLS of the TP/SASM, so the missing of NAT mechanism in the GEOS-Chem model should not compromise the conclusion of our study. We have added a sentence to discuss NAT at the end of the conclusion section.

4. In addition to the reaction of nitric acid with ammonia, as stated in the

manuscript (Line244-245), nitrate aerosol can also form by multi-phase chemistry including mineral and sea salt aerosols, even in the free troposphere over TP (Ma et al., 2003). Previous studies showed that mineral dust could make a considerable contribution to elevated summertime aerosol concentrations in the UTLS over the TP/SASM region (Fadnavis et al., 2013). While it is stated that mineral dust aerosols are included in GEOS-Chem (Line 177-181), they are neither presented nor discussed in the manuscript.

Response:

We agree with the reviewer that nitrate aerosol can also form by multi-phase chemistry on mineral and sea salt aerosols (Ma et al., 2003; Liao et al., 2004). The GEOS-Chem model uses the aerosol thermodynamic equilibrium module ISORROPIA to calculate concentrations of nitrate, which accounts for the formation of ammonium nitrate and the formation of nitrate on sea salt aerosol. However, the formation of nitrate on mineral dust aerosol is not considered in the publicly released versions of the GEOS-Chem model. Fadnavis et al. (2013) showed, by using the ECHAM5-HAMMOZ model, that mineral dust aerosol contributed to the enhanced aerosol extinction in the UTLS over the anticyclone region during summer. Their simulated seasonal mean concentrations of mineral dust were $0.010–0.029$ μg m^{-3} at 110 hPa over the TP/SASM region in summer of 2003. The upper end of their simulated mineral dust concentration is close to the simulated SO_4^{2-} concentration at 100 hPa in our work. We have added a sentence at the end of the conclusion section to clarify that future studies need to account for mineral dust aerosol.

5. In this study simulated O_3 profiles are compared with balloon-borne sonde measurements at Kunming in August 2009 and at Lhasa in August 2010 (337-350). How frequent were O_3 profiles measured at these two sites? Are there sufficient measured O_3 profiles for calculating the monthly mean values for comparison?

Response:

The measurements used in the comparisons were 11 profiles of O_3 in Kunming over August 7–13, 2009, and 12 profiles of O_3 in Lhasa over August 22–28, 2010, which should be enough for calculating the monthly mean O_3 values. To help with our argument, we have added in Figure 6 the monthly mean O_3 profile obtained from daily observations in Kunming during August 12–31, 2012, and the monthly mean O_3 profile obtained from the daily observations in Lhasa during August 4–26, 2013. The updated Figure 6 is shown below.

We have revised Section 3.2 accordingly: "In addition to the comparisons against MLS products, the simulated O_3 profiles are compared with balloon-borne sonde measurements in Fig. 6. The measurements were carried out at Kunming (KM, 102.7°E, 25.0°N) in August of 2009 and 2012, and at Lhasa (LH, 91.1°E, 29.7°N) in August of 2010 and 2013. The uncertainties of the observed O_3 mixing ratios were estimated to be within 5–10% (Bian et al. 2012). The comparisons with multi-year observations show that the model can reproduce the vertical distributions of O_3 in Kunming and Lhasa. At 100 hPa, the simulated monthly mean O_3 mixing ratio in KM is 112.6 ppbv, and the observed value is 124.2 ppbv in 2009 and 113.5 ppbv in 2012. In LH, the simulated monthly O_3 mixing ratio at 100 hPa is 152.6 ppbv, and the observed O_3 mixing ratio at that altitude is 142.4 ppbv in 2010 and 167.9 ppbv in 2013.

The magnitudes of O_3 mixing ratios from these balloon-borne sonde measurements support those from MLS; O_3 mixing ratios in the UTLS are less than 200 ppbv over the TP/SASM region."
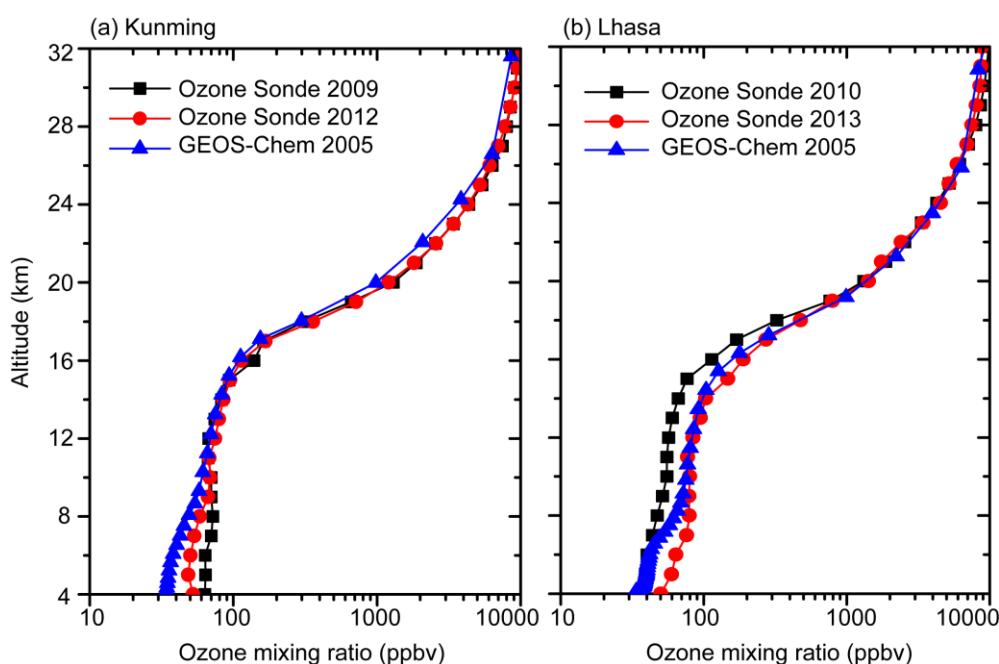

Figure 6. The simulated and observed vertical profiles of monthly mean O_3 mixing ratios at (a) Kunming and (b) Lhasa in August. The model results are from the simulation of year 2005. The observations in Kunming were conducted during August 7−13 (11 profiles of O_3 collected) in 2009 and during August 12−31 in 2012 (daily observations). The observations in Lhasa were conducted during August 22−28 in 2010 (12 profiles of O_3 collected) and during August 4−26 in 2013 (daily observations).

6. Also for model evaluation, the observed PM_{10} concentrations were converted to $PM_{2.5}$, following the suggestions of Zhang et al. (2002) (Line 398-399). Is that work of Zhang et al. (2002) related to $PM_{2.5}$ and PM_{10} in the TP/SASM region? The authors are suggested to consider referring to measurement work in the investigated region.
Response:
    The observations in Zhang et al. (2002) were conducted in Xi'an in northwestern China. Chatterjee et al. (2010) measured aerosol concentrations in Darjeeling, a station in northeastern Himalayas, during January-December of 2005, and reported that fine aerosol ($PM_{2.5}$) concentration accounted for 58.3% of PM_{10} concentration on average. Therefore it is OK to use the factor of 0.6 from Zhang et al. (2002) to convert PM_{10} to $PM_{2.5}$ for the TP/SASM region. We have revised this sentence as: "The observed PM_{10} concentrations listed in Table S1 are multiplied by 0.6 to convert to $PM_{2.5}$ for model evaluation, following the suggestions in Zhang et al. (2002) and Chatterjee et al. (2010)."

7. With respect to the hygroscopic growth of aerosols (432-434), are the growth factors calculated on-line for internal-mixed aerosols in GEOS-Chem? It is stated that the region with relatively high aerosols extinction coefficients (Fig. 9) corresponds to that with high $PM_{2.5}$ concentrations at 100 hPa (Fig.7)

(Line 435-438). This statement might not be true if one would compare the two plots carefully.

Response:

(1) Yes. It is clarified in Section 4.3: "The hygroscopic growth of each aerosol species with relative humidity is accounted for, using the hygroscopic growth factors listed in Martin et al. (2003)".

(2) Thanks for pointing this out. At 100 hPa, the simulated $PM_{2.5}$ concentrations are high over the anticyclone region, with peak values near the south slop of the Himalayas. The simulated aerosol extinction coefficients are also high over the anticyclone region, but the peak values extend to the Arabian Peninsula and the nearby ocean. The reasons for the differences are as follows. While simulated $PM_{2.5}$ considers only sulfate, nitrate, ammonium, OC and BC aerosols, simulated aerosol extinction coefficient accounts for the contributions of sulfate, nitrate, ammonium, OC, sea salt, and mineral dust to compare with SAGEII measurements. Mineral dust aerosol has been shown to contribute largely to elevated summertime aerosols in the UTLS over the Asian summer monsoon region, especially over the Arabian Peninsula and the nearby ocean (Fadnavis et al., 2013). We have revised the sentence as: "At 100 hPa, the simulated aerosol extinction coefficients are relatively high over the anticyclone region, where anthropogenic aerosol species (Fig. 7) and natural aerosols such as mineral dust and sea salt contribute to aerosol extinction coefficients in summer".

8. Line175: 34 layers in the troposphere?

Response:

Yes.

9. Line 279: Fig. 4(a) and Fig. 4(b)?

Response:

We have changed "Fig. 3(a) and Fig. 3(b)" to "Fig. 4(a) and Fig. 4(b)".

10. Line 529: Fig. 12(c)?

Response:

We have changed "Fig. 13(c)" to "Fig. 12(c)".

11. There are several literatures listed in the References but not cited in the formal text.

References

Fadnavis, S., Semeniuk, K., Pozzoli, L., Schultz, M. G., Ghude, S. D., Das, S., and Kakatkar, R.: Transport of aerosols into the UTLS and their impact on the Asian monsoon region as seen in a global model simulation, Atmos. Chem. Phys., 13, 8771-8786,10.5194/acp-13-8771-2013, 2013.

Kirner, O., Ruhnke, R., Buchholz-Dietsch, J., Jöckel, P., Brühl, C., and Steil, B.: Simulation of polar stratospheric clouds in the chemistry-climate-model EMAC via the submodel PSC, Geosci. Model Dev., 4, 169-182, 10.5194/gmd-4-169-2011, 2011.

Ma, J., Tang, J., Li, S.-M., and Jacobson, M. Z.: Size distributions of ionic

aerosols measured at Waliguan Observatory: Implication for nitrate gas-to-particle transfer processes in the free troposphere, J. Geophys. Res., 108, 4541, 10.1029/2002jd003356, 2003.

Zhang, X., Cao, J., Li, L., Arimoto, R., Cheng, Y., Huebert, B., and Wang, D.: Characterization of atmospheric aerosol over Xian in the south margin of the Loess Plateau, China, Atmos.Environ., 36, 4189–4199, 2002.

Response:
    We have included these studies in our reference list.

References:
Bian, J., Pan, L. L., Paulik, L., Vömel, H., Chen, H., and Lü, D.: In situ water vapor and ozone measurements in Lhasa and Kunming during the Asian summer monsoon, Geophys. Res. Lett., 39, L19808, doi:10.1029/2012GL052996, 2012.
Carslaw, K., Wirth, M., Tsias, A., Luo, B., Dörnbrack, A., Leutbecher, M., Volkert, H., Renger, W., Bacmeister, J., and Peter, T.: Particle microphysics and chemistry in remotely observed mountain polar stratospheric clouds, J. Geophys. Res., 103, 5785–5796, 1998.
Chatterjee, A., Adak, A., Singh, A. K., Srivastava, M. K., Ghosh, S. K., Tiwari, S., Devara, P. C., and Raha, S.: Aerosol chemistry over a high altitude station at northeastern Himalayas, India, PloS one, 5, e11122, 2010.
Considine, D. B., Logan, J. A., and Olsen, M. A.: Evaluation of near-tropopause ozone distributions in the Global Modeling Initiative combined stratosphere/troposphere model with ozonesonde data, Atmos. Chem. Phys., 8, 2365–2385, 2008.
Dawson, J., Adams, P., and Pandis, S.: Sensitivity of $PM_{2.5}$ to climate in the Eastern US: a modeling case study, Atmos. Chem. and phys., 7, 4295–4309, 2007.
Duncan, B., Strahan, S., Yoshida, Y., Steenrod, S., and Livesey, N.: Model study of the cross-tropopause transport of biomass burning pollution, Atmos. Chem. Phys., 7, 3713–3736, 2007.
Fadnavis, S., Semeniuk, K., Pozzoli, L., Schultz, M. G., Ghude, S. D., Das, S., and Kakatkar, R.: Transport of aerosols into the UTLS and their impact on the Asian monsoon region as seen in a global model simulation, Atmos. Chem. Phys., 13, 8771-8786,10.5194/acp-13-8771-2013, 2013.
Fiorucci, I., Muscari, G., Froidevaux, L., and Santee, M. L.: Ground-based stratospheric O_3 and HNO_3 measurements at Thule, Greenland: an intercomparison with Aura MLS observations, Atmospheric Measurement Techniques Discussions, 6(2), 2441-2453, doi:10.5194/amt-6-2441-2013, 2013.
Fountoukis, C., and Nenes, A.: ISORROPIA II: a computationally efficient thermodynamic equilibrium model for K^+–Ca^{2+}–Mg^{2+}–NH_4^+–Na^+–SO_4^{2-}–NO_3^-–Cl^-–H_2O aerosols, Atmos. Chem. Phys., 7, 4639–4659, 2007.
Hofmann, D., Rosen, J., Harder, J., and Hereford, J.: Balloon-borne measurements of aerosol, condensation nuclei, and cloud particles in the stratosphere at McMurdo Station, Antarctica, during the spring of

1987, J. Geophys. Res., 94, 11253–11269, doi:10.1029/JD094iD09p11253, 1989.

Jiang, H., Liao, H., Pye, H., Wu, S., Mickley, L. J., Seinfeld, J. H., and Zhang, X.: Projected effect of 2000–2050 changes in climate and emissions on aerosol levels in China and associated transboundary transport, Atmos. Chem. Phys., 13, 7937–7960, 2013.

Kim, Y.- S., Shibata, T., Iwasaka, Y., Shi, G., Zhou, X., Tamura, K., and Ohashi, T.: Enhancement of aerosols near the cold tropopause in summer over Tibetan Plateau: lidar and balloonborne measurements in 1999 at Lhasa, Tibet, China, in: Lidar Remote Sensing for Industry and Environment Monitoring III, edited by: Singh U. N., Itabe, T., and Liu, Z., Proceedings of SPIE, Hangzhou, China, 4893, 496–503, 2003.

Kirner, O., Ruhnke, R., Buchholz-Dietsch, J., Jöckel, P., Brühl, C., and Steil, B.: Simulation of polar stratospheric clouds in the chemistry-climate-model EMAC via the submodel PSC, Geosci. Model Dev., 4, 169-182, doi:10.5194/gmd-4-169-2011, 2011.

Li, Q., Jiang, J. H., Wu, D. L., Read, W. G., Livesey, N. J., Waters, J. W., Zhang, Y., Wang, B., Filipiak, M. J., and Davis, C. P.: Convective outflow of South Asian pollution: A global CTM simulation compared with EOS MLS observations, Geophys. Res. Lett., 32, L14826, doi:10.1029/2005GL022762, 2005.

Liao, H., Seinfeld, J. H., Adams, P. J., and Mickley L. J.: Global radiative forcing of coupled tropospheric ozone and aerosols in a unified general circulation model, J. Geophys. Res., 109, D16207, doi:10.1029/2003JD004456, 2004.

Liao, H., and Seinfeld J. H.: Global impacts of gas-phase chemistry-aerosol interactions on direct radiative forcing by anthropogenic aerosols and ozone, J. Geophys. Res., 110, D18208, doi:10.1029/2005JD005907, 2005.

Liao, H., Zhang, Y., Chen, W.-T., Raes, F., and Seinfeld, J. H.: Effect of chemistry-aerosol-climate coupling on predictions of future climate and future levels of tropospheric ozone and aerosols, J. Geophys. Res., 114, D10306, doi:10.1029/2008JD010984, 2009.

Livesey, N. J., Read, W. G., Wagner, P. A., Froidevaux, L., Lambert, A., Manney, G. L., Pumphrey, H. C., Santee, M. L., Schwartz, M. J., Wang, S., Cofield, R. E., Cuddy, D. T., Fuller, R. A., Jarnot, R. F., Jiang, J. H., and Knosp, B. W.: Version 3.3 Level 2 data quality and description document, JPL D-33509, 2011.

Lou, S., Liao, H., and Zhu, B.: Impacts of aerosols on surface-layer ozone concentrations in China through heterogeneous reactions and changes in photolysis rates, Atmos. Environ., 85, 123–138, 2014.

Ma, J., Tang, J., Li, S.-M., and Jacobson, M. Z.: Size distributions of ionic aerosols measured at Waliguan Observatory: Implication for nitrate gas-to-particle transfer processes in the free troposphere, J. Geophys. Res., 108, 4541, doi:10.1029/2002jd003356, 2003.

Martin, R. V., Jacob, D. J., Yantosca, R. M., Chin, M., and Ginoux, P.: Global and regional decreases in tropospheric oxidants from photochemical effects of aerosols, J. Geophys. Res., 108, 4097, doi:10.1029/2002JD002622, 2003.

Miyazaki, K., Eskes, H. J., Sudo, K., Takigawa, M., van Weele, M., and

Boersma, K. F.: Simultaneous assimilation of satellite NO_2, O_3, CO, and HNO_3 data for the analysis of tropospheric chemical composition and emissions, Atmos. Chem. Phys., 12, 9545–9579, doi:10.5194/acp-12-9545-2012, 2012.

Murray, L. T., Jacob, D. J., Logan, J. A., Hudman, R. C., and Koshak, W. J.: Optimized regional and interannual variability of lightning in a global chemical transport model constrained by LIS/OTD satellite data, J. Geophys. Res., 117, D20307, doi:10.1029/2012JD017934, 2012.

Park, R. J., Jacob, D. J., Field, B. D., Yantosca, R. M., and Chin, M.: Natural and transboundary pollution influences on sulfate-nitrate-ammonium aerosols in the United States: Implications for policy, J. Geophys. Res., 109, D15204, doi:10.1029/2003JD004473, 2004.

Popp, P., Marcy, T., Jensen, E., Kärcher, B., Fahey, D., Gao, R., Thompson, T., Rosenlof, K., Richard, E., and Herman, R.: The observation of nitric acid-containing particles in the tropical lower stratosphere, Atmos. Chem. Phys., 6, 601-611, 2006.

Pye, H., Liao, H., Wu, S., Mickley, L. J., Jacob, D. J., Henze, D. K., and Seinfeld, J.: Effect of changes in climate and emissions on future sulfate–nitrate–ammonium aerosol levels in the United States, J. Geophys. Res., 114, D01205, doi:10.1029/2008JD010701, 2009.

Seinfeld, J. H., and Pandis, S. N.: Atmospheric chemistry and physics: from air pollution to climate change, Environment Science & Policy for Sustainable Development, 51, 212–214(213), 2006.

Schwartz, M. J., Manney, G. L., Hegglin, M. I., Livesey, N. J., Santee, M. L., and Daffer, W. H.: Climatology and variability of trace gases in extratropical double-tropopause regions from MLS, HIRDLS, and ACE-FTS measurements, J. Geophys. Res. Atmos., 120, 843–867, doi:10.1002/2014JD021964, 2015.

Tobo, Y., Zhang, D., Iwasaka, Y., and Shi, G.: On the mixture of aerosols and ice clouds over the Tibetan Plateau: Results of a balloon flight in the summer of 1999, Geophys. Res. Lett., 34, L23801, doi:10.1029/2007GL031132, 2007.

Voigt, C., Schreiner, J., Kohlmann, A., Zink, P., Mauersberger, K., Larsen, N., Deshler, T., Kröger, C., Rosen, J., and Adriani, A.: Nitric acid trihydrate (NAT) in polar stratospheric clouds, Science, 290, 1756-1758, 2000.

Yan, X. L., Zheng, X. D., Zhou, X. J., VÖMEL, H., Song, J. Y., Li, W., Ma, Y. H., Zhang, Y.: Validation of Aura Microwave Limb Sounder water vapor and ozone profiles over the Tibetan Plateau and its adjacent region during boreal summer. Science China: Earth Sciences, 58: 589–603, doi:10.1007/s11430-014-5014-1, 2015.

Yao, X., Chan, C. K., Fang, M., Cadle, S., Chan, T., Mulawa, P., He, K., and Ye, B.: The water-soluble ionic composition of $PM_{2.5}$ in Shanghai and Beijing, China, Atmos. Environ., 36, 4223–4234, 2002.

Zhang, L., Liao, H. and Li, J.: Impacts of Asian summer monsoon on seasonal and interannual variations of aerosols over eastern China, J. Geophys. Res., 115, D00K05, doi:10.1029/2009JD012299, 2010.

Zhang, X., Cao, J., Li, L., Arimoto, R., Cheng, Y., Huebert, B., and Wang, D.: Characterization of atmospheric aerosol over Xian in the south margin of the Loess Plateau, China, Atmos.Environ., 36, 4189–4199, 2002.

Zhang, X. Y., Wang, Y. Q., Niu, T., Zhang, X. C., Gong, S. L., Zhang, Y. M., and

Sun, J. Y.: Atmospheric aerosol compositions in China: spatial/temporal variability, chemical signature, regional haze distribution and comparisons with global aerosols, Atmos. Chem. Phys., 12, 779–799, doi:10.5194/acp-12-779-2012, 2012.

Zhu, J., Liao, H., and Li, J.: Increases in aerosol concentrations over eastern China due to the decadal-scale weakening of the East Asian summer monsoon, Geophys. Res. Lett., 39, L09809, doi:10.1029/2012GL051428, 2012.

1 Summertime nitrate aerosol in the upper troposphere and lower stratosphere

2 over the Tibetan Plateau and the South Asian summer monsoon region

3

4

5

6

7 Yixuan Gu[a,b], Hong Liao[a,*], and Jianchun Bian[c]

8

9 [a]State Key Laboratory of Atmospheric Boundary Layer Physics and

10 Atmospheric Chemistry (LAPC), Institute of Atmospheric Physics, Chinese

11 Academy of Sciences, Beijing, China.

12 [b]University of Chinese Academy of Sciences, Beijing, China

13 [c]Key Laboratory of Middle Atmosphere and Global Environment Observation

14 (LAGEO), Institute of Atmospheric Physics, Chinese Academy of Sciences,

15 Beijing, China.

16

17

18

19

20 *Corresponding author address:

21 Prof. Hong Liao

22 LAPC, Institute of Atmospheric Physics

23 Chinese Academy of Sciences

24 Beijing 100029, China

25 E-mail: hongliao@mail.iap.ac.cn

Abstract

We use the global three-dimensional Goddard Earth Observing System chemical transport model (GEOS-Chem) to examine the contribution of nitrate aerosol to aerosol concentrations in the upper troposphere and lower stratosphere (UTLS) over the Tibetan Plateau and the South Asian summer monsoon (TP/SASM) region during summertime of year 2005. Simulated surface-layer aerosol concentrations are compared with ground-based observations, and simulated aerosols in the UTLS are evaluated by using the Stratospheric Aerosol and Gas Experiment II satellite data. Simulations show elevated aerosol concentrations of sulfate, nitrate, ammonium, black carbon, organic carbon, and PM$_{2.5}$ (particles with diameter equal or less than 2.5 μm, the sum of sulfate, nitrate, ammonium, black carbon, and organic carbon aerosols) in the UTLS over the TP/SASM region throughout the summer. Nitrate aerosol is simulated to be of secondary importance near the surface but the most dominant aerosol species in the UTLS over the studied region. Averaged over summertime and over the TP/SASM region, C$_{NIT}$ (the ratio of nitrate concentration to PM$_{2.5}$ concentration) values are 5–35% at the surface, 25–50% at 200 hPa, and could exceed 60% at 100 hPa. The mechanisms for the accumulation of nitrate in the UTLS over the TP/SASM region include vertical transport and the gas-to-aerosol conversion of HNO$_3$ to form nitrate. The high relative humidity and low temperature associated with the deep convection over the TP/SASM region are favorable for the gas-to-aerosol conversion of HNO$_3$.

1 Introduction

Aerosols in the upper troposphere and lower stratosphere (UTLS) have much longer residence times than those in the lower troposphere, influencing atmospheric chemistry and the Earth's climate with large spatial and temporal coverage (Rasch et al., 2008). Aerosols in the UTLS influence the concentrations of chemical species via changes in photolysis rates and heterogeneous reactions (Pitari et al., 2014). For example, heterogeneous reactions on sulfate aerosol can perturb the chemical partitioning in the lower stratosphere, leading to significant O_3 depletion through enhanced chlorine, bromine, and odd-hydrogen catalytic cycle (Zhao et al., 1997; Considine et al., 2001; Talukdar et al., 2012; Tang et al., 2014; Pitari et al., 2014). Aerosols in the UTLS also influence climate by altering properties of cirrus clouds via homogeneous or heterogeneous ice nucleation (Li et al., 2005; Liu et al., 2009; Yin et al., 2012; Fadnavis et al., 2013). Injection of aerosols into the UTLS has been reported to induce complex responses in circulation, temperature, and water vapor (Liu et al., 2009; Wu et al., 2011; Su et al., 2011; Fadnavis et al., 2013).

Aerosols over the Tibetan Plateau (TP) and the Asian summer monsoon region are especially important. The TP is surrounded by countries with large anthropogenic emissions (Li et al., 2005; Lau et al., 2006). Aerosols from India, Southeast Asia, and southern China can be transported to the TP by prevailing winds in the premonsoon and monsoon seasons (Lawrence and Lelieveld, 2010; Xia et al., 2011). Observational and modeling studies have shown that persistent maxima of atmospheric constituents, such as water vapor (Gettelman et al., 2004; Randel and Park, 2006; Park et al., 2007), CO (Kar et

74 al., 2004; Li et al., 2005; Park et al., 2007, 2008, 2009), CH_4 (M. Park et al.,

75 2004; Xiong et al., 2009), NO_x (M. Park et al., 2004), HCN (Park et al., 2008;

76 Randel et al., 2010), C_2H_6 and C_2H_2 (Park et al., 2008), exist in the UTLS

77 above the TP and the South Asian summer monsoon (SASM) region because

78 of the deep convection during boreal summer. Satellite observations

79 suggested that the convection associated with the SASM is a vital pathway to

80 transport air mass from the lower troposphere into the stratosphere (Chen et

81 al., 2006; Randel and Park, 2006; Randel et al., 2010; Bian et al., 2011a). The

82 heating associated with the persistent deep convection during summertime

83 leads to the formation of the Tibetan anticyclone in the UTLS, which acts to

84 isolate air within the anticyclone and traps the uplifted pollutants at that altitude

85 (Park et al., 2007; Vernier et al., 2011; Bourgeois et al., 2012; Fadnavis et al.,

86 2013; He et al., 2014). The stratosphere-troposphere exchange (STE) over the

87 TP contributes largely to the global STE (Chen et al., 2006).

88   Previous studies have reported that aerosols exist in the UTLS over the

89 TP/SASM region. Kim et al. (2003) carried out optical measurements with a

90 ground-based lidar in Lhasa from August to October of 1999, and found an

91 enhancement in aerosol concentration near the local tropopause with

92 scattering ratio (SR, the ratio of aerosol plus molecular backscatter to

93 molecular backscatter alone) of 1.1−1.2. Tobo et al. (2007) reported an

94 enhancement of sub-micron aerosols (effective radius r = 0.15−0.6 μm) near

95 the summertime tropopause (about 130 to 70 hPa), on the basis of in situ

96 balloon measurements from an Optical Particle Counter at the same location in

97 August of 1999. Vernier et al. (2009) examined satellite measurements from

98 the Cloud-Aerosol Lidar with Orthogonal Polarization (CALIOP) onboard

99   Cloud-Aerosol Lidar and Infrared Pathfinder Satellite Observation (CALIPSO)

100   and reported the presence of small depolarizing particles with high SR values

101   (about 1.20 at 532 nm) at 16−17 km altitude over South Asia in July and

102   August of 2007 and 2008. Bourgeois et al. (2012) found that an aerosol layer

103   existed at 16−18 km altitude over the Asian continent and Indian Ocean

104   (20°S−30°N, 5−105°E) on the basis of the CALIOP observations. Recently, He

105   et al. (2014) examined the vertical profiles of aerosol extinction coefficients

106   measured with a Micro Pulse Lidar at Naqu, a meteorological station located in

107   the central part of the TP, and also showed a maximum in aerosol extinction

108   coefficient ($\sim 2.10^{-3}$ km^{-1}) in the UTLS (18−19 km) during the summer of 2011.

109   A number of previous studies have attempted to understand the chemical

110   composition of aerosols in the UTLS. Froyd et al. (2009) measured aerosol

111   composition with the National Oceanic and Atmospheric Administration (NOAA)

112   single-particle mass spectrometer aboard the National Aeronautics and Space

113   Administration (NASA) WB-57 high altitude aircraft platform, and reported that

114   particles in the tropical tropopause layer were rich in nitrogen. Vernier et al.

115   (2011) suggested that aerosol layer at the tropopause of Asia could be sulfur

116   and/or organics, considering that Asian pollutants consisted of black carbon,

117   organic carbon, SO_2, and NO_x (Park et al., 2009; Randel et al., 2010). Weigel

118   et al. (2011) analyzed the volatility of aerosols obtained from in situ airborne

119   measurements and reported that about 75–90 % of the particles in the tropical

120   tropopause layer were volatile, but this study did not give any detailed

121   analyses of chemical composition of aerosols. Bourgeois et al. (2012) showed,

122   by using the ECHAM5.5-HAM2 model, that sulfate, water, and OC contributed,

123   respectively, 53%, 29%, and 11% to aerosol extinction in the vicinity of the

124 tropical tropopause layer. The ECHAM5.5-HAM2 model used by Bourgeois et

125 al. (2012) simulated all major aerosol species in the atmosphere except for

126 nitrate.

127 Few previous studies have examined nitrate aerosol in the UTLS, although

128 nitrate is expected to be important for the following reasons. First, emissions of

129 precursors of nitrate, such as NO_x and NH_3, are high over India, Southeast

130 Asia, and China (Streets et al., 2003; Datta et al., 2012; Huang et al., 2012).

131 Second, simulated nitrate concentrations are high over those regions (Liao and

132 Seinfeld, 2005; Mu and Liao, 2014; Lou et al., 2014). Third, measured

133 concentrations of nitrate are comparable to or larger than those of sulfate at

134 rural and urban sites in the SASM region. Shrestha et al. (2000) carried out

135 measurements of aerosols at Phortse, Nepal, during September

136 1996−November 1997, and showed that the average concentration of nitrate

137 during the monsoon season (June-September) was 0.34 μg m^{-3}, higher than

138 that of sulfate (0.17 μg m^{-3}). Decesari et al. (2010) reported, on the basis of

139 measurements at the Nepal Climate Observatory-Pyramid from 2006 to 2008,

140 that the concentrations of nitrate and sulfate were 0.37 μg m^{-3} and 0.50 μg m^{-3},

141 respectively, during the monsoon season. Chatterjee et al. (2010) measured

142 aerosols at a high altitude station in northeastern Himalayas during

143 January-December 2005. They found that the average concentrations of

144 fine-mode nitrate and sulfate were 3.31±2.25 μg m^{-3} and 3.80±2.9 μg m^{-3},

145 respectively. At Lahore, an urban site in Pakistan, the observed daytime nitrate

146 concentration of 21.8 μg m^{-3} was also higher than sulfate concentration of 12.6

147 μg m^{-3} (Lodhi et al., 2009), as the observations were averaged over November

148 2005 to March 2006. Fourth, the low temperatures in the UTLS would favor

149 nitrate formation (Seinfeld and Pandis, 2006). Therefore, it is of interest to take

150 nitrate aerosol into consideration when we examine aerosols in the UTLS.

151   In this work we simulate nitrate aerosol and its contribution to aerosol

152 concentrations in the UTLS over the TP (70–105°E, 25–40°N) and the SASM

153 region (70–105°E, 10–25°N) by using the global chemical transport model

154 GEOS-Chem driven by the assimilated meteorological fields. These regions of

155 interest are shown in Fig. 1. Simulated surface-layer aerosol concentrations

156 are compared with ground-based observations, and simulated aerosols in the

157 UTLS are evaluated by using the Stratospheric Aerosol and Gas Experiment

158 II (SAGE II) satellite data. Section 2 is a brief description of the GEOS-Chem

159 model and numerical experiment. Section 3 presents the simulation and

160 evaluation of distributions and concentrations of HNO_3 and O_3 to show model's

161 capability in simulating the NO_x-O_3-HNO_3 cycle over the studied regions.

162 Section 4 shows simulated aerosols and Section 5 presents the simulated

163 contribution of nitrate to aerosol concentrations in the UTLS over the TP and

164 the SASM region. Section 6 discusses the mechanisms for high concentrations

165 of nitrate in the UTLS. Section 7 discusses the impacts of uncertainties in

166 surface-layer aerosol concentrations on simulated nitrate in the UTLS.

167

168 **2 Model description and numerical experiment**

169 **2.1 GEOS-Chem model**

170 We simulate gas-phase species and aerosols using the global chemical

171 transport model GEOS-Chem (version 9-01-03,

172 http://acmg.seas.harvard.edu/geos/index.html) driven by the GEOS-5

173 assimilated meteorological fields from the Goddard Earth Observing System of

the NASA Global Modeling and Assimilation Office. The version of the model used here has a horizontal resolution of 2° latitude by 2.5° longitude and 47 vertical layers extending from the surface to 0.01 hPa. Over the TP and the SASM region, the model has about 34 layers in the troposphere and 12 layers in the stratosphere.

The GEOS-Chem model has a fully coupled treatment of tropospheric NO_x-CO-hydrocarbon-aerosol chemistry and aerosols including sulfate (SO_4^{2-}), nitrate (NO_3^-), ammonium (NH_4^+), organic carbon (OC), black carbon (BC) (R. J. Park et al., 2003; 2004; Pye et al., 2009), mineral dust (Fairlie et al., 2007), and sea salt (Alexander et al., 2005; Jaeglé et al., 2011). The gas-aerosol partitioning of nitric acid and ammonium is calculated using the ISORROPIA II thermodynamic equilibrium module (Fountoukis and Nenes, 2007). The two-way coupling between aerosols and gas phase chemistry provides consistent chemical fields for aerosol simulation and aerosol mass for heterogeneous processes and calculations of gas-phase photolysis rates. Heterogeneous reactions include hydrolysis of N_2O_5 (Evans and Jacob, 2005), irreversible absorption of NO_3 and NO_2 on wet aerosols (Jacob, 2000), and the uptake of HO_2 by aerosols (Liao and Seinfeld, 2005; Thornton et al., 2008).

With respect to chemistry in the stratosphere, stratospheric O_3 concentrations are calculated using the linearized parameterization scheme (McLinden et al., 2000). The monthly mean production rates and loss frequencies of other stratospheric species (including long-lived species such as CFCs and N_2O) use those from NASA Global Modeling Initiative (GMI) Combo simulations (Duncan et al., 2007; Considine et al., 2008; Murray et al., 2012).

199   Convective transport in GEOS-Chem mimics that in the parent GEOS

200   general circulation model (GCM) (Hack, 1994; Zhang and McFarlane, 1995),

201   which accounts for updraft, downdraft, and entrainment mass fluxes for deep

202   and shallow convection (Wu et al., 2007). The aerosol wet deposition scheme

203   in the GEOS-Chem follows that of Liu et al. (2001). For the scavenging of

204   aerosols, SO_4^{2-}, NO_3^-, NH_4^+, and hydrophilic OC and BC aerosols are assumed

205   to be fully soluble. Dry deposition follows the standard resistance-in-series

206   model of Wesely (1989).

207   Global emissions of aerosols and their precursors in the GEOS-Chem

208   follow R. J. Park et al. (2003, 2004), with anthropogenic emissions of NO_x, CO,

209   SO_2, and non-methane volatile organic compounds (NMVOC) in Asia

210   overwritten   by   David   Streets'   2006   emission   inventory

211   (http://mic.greenresource.cn/intex-b2006). Emissions of NH_3 in Asia are taken

212   from Streets et al. (2003). Since NH_3 emissions in China showed large

213   uncertainties in previous studies (Streets et al., 2003; Kim et al., 2006; Y.

214   Zhang et al., 2010; Huang et al., 2011, 2012), we use the most recent estimate

215   of NH_3 emissions in China by Huang et al. (2012), which is 9.8 Tg yr^{-1}, instead

216   of 13.5 Tg yr^{-1} from Streets et al. (2003). Table 1 summarizes the annual

217   emissions of NO_x, SO_2, NH_3, OC, and BC in Asia domain (60−155°E,

218   10−55°N).

219   Natural NO_x emissions from lightning are calculated using the scheme

220   described by Sauvage et al. (2007) and Murray et al. (2012), and those from

221   soil are simulated following Wang et al. (1998). Natural NH_3 emissions from

222   soil, vegetation, and the oceans are taken from the Global Emissions Inventory

223   Activity inventory (Bouwman et al., 1997). Biomass burning emissions are from

the monthly Global Fire Emissions Database (GFED v3) driven by satellite observations of fire activity (van der Werf et al., 2010). Biogenic VOC (volatile organic compounds) emissions are calculated from the Model of Emissions of Gases and Aerosols from Nature (Guenther et al., 2006).

The monthly variations of emissions of SO_2 and NO_x follow Wang et al. (2013) and those of BC and OC follow Lou et al. (2014). The monthly scaling factors for NH_3 emissions follow the global inventory compiled by Marcel Meinders and Lex Bouwman (Fisher et al., 2011). Monthly variations of emissions (anthropogenic plus natural emissions) of NO_x SO_2, NH_3, OC, and BC over Asia are displayed in Fig. 2. The emissions of NH_3 are the highest in June as a result of the agriculture practice and high temperatures (Wang et al., 2013).

2.2 Numerical experiment

To examine the contribution of nitrate to aerosol concentrations in the UTLS over the TP/SASM region, we simulate aerosol concentrations by using the emissions of and meteorological fields of year 2005. Year 2005 is chosen so that we can use the observational datasets for this year from SAGE II and MLS, as described in Sects. 3 and 4. Following Rasch et al. (2008), we perform a 10-year spin-up run to generate the initial conditions (to allow the stratospheric species to reach quasi-steady state conditions). We would consider that the tropospheric simulation can be representative of year 2005 but stratosphere simulation should represent a multi-year average, because the production rates and loss frequencies in the stratosphere are the averages over years of 2004−2010 (http://wiki.seas.harvard.edu/geos-chem/index.php/ Stratospheric_ chemistry).

249

3 Simulated concentrations of HNO$_3$ and O$_3$ and model evaluation

250 Nitrate aerosol forms when nitric acid (HNO$_3$) reacts with alkaline gases (for

251

252 example, ammonia) in the atmosphere (Seinfeld and Pandis, 2006). HNO$_3$, as

253 the important precursor of nitrate, is the major oxidation product of nitrogen

254 oxides (NO$_x$ = NO+NO$_2$) (Seinfeld and Pandis, 2006). To show the model's

255 capability in simulating the NO$_x$-O$_3$-HNO$_3$ cycle over the studied regions, we

256 present and evaluate the simulated HNO$_3$ and O$_3$ in this section.

257 Simulated mixing ratios of HNO$_3$ and O$_3$ in the UTLS are evaluated by

258 using datasets from the limb viewing satellite instrument of Microwave Limb

259 Sounder (MLS, version 3.3, level 2,

260 ftp://acdisc.gsfc.nasa.gov/data/s4pa///Aura_MLS_Level2/). The MLS datasets

261 provide valuable information on atmospheric compositions in the UTLS

262 (Waters et al., 2006). For HNO$_3$, the MLS provides datasets for 215 to 1.5 hPa,

263 with a vertical resolution of 3−4 km and a horizontal resolution of 400−500 km.

264 Since further evaluations are needed for datasets at altitudes with pressures

265 higher than 215 hPa (Livesey et al., 2011), we use only datasets for pressures

266 lower than that. For O$_3$, the MLS provides datasets for 261 to 0.02 hPa, with a

267 vertical resolution of 2.5−3 km and a horizontal resolution of 300−400 km in the

268 UTLS (Santee et al., 2007; Livesey et al., 2011). The uncertainties of the MLS

269 HNO$_3$ and O$_3$ datasets in the UTLS are about ±0.5−1 ppbv (± 5−10%) and

270 0.02−0.04 ppmv, respectively (Livesey et al., 2011).

271 **3.1 HNO$_3$**

272 Figure 3(a) shows the simulated global distribution of HNO$_3$ concentrations

273 averaged over June-August of 2005. Concentrations of HNO$_3$ exceed 1 ppbv

over the industrialized areas such as Europe, North America, central and eastern Asia, and over biomass burning regions in the tropics, in agreement with the distributions and magnitudes reported in Liao et al. (2003). Over South Asia, simulated HNO_3 concentrations are high (0.3−1 ppbv) in the northern Indian subcontinent, because the emissions of NO_x and NH_3 are high in this region (Streets et al., 2003; Zhang et al., 2009; Datta et al., 2012).

Figures 4(a)-4(b) show the simulated HNO_3 concentrations in the UTLS averaged over June-August of 2005. Since the tropopause is located at 70−150 hPa (12−15 km) over the TP/SASM region (Li et al., 2005; Bian et al., 2011b; Fadnavis et al., 2014), we choose the vertical layers of 200 hPa and 100 hPa to represent the UTLS. At both 200 hPa and 100 hPa, the highest HNO_3 concentrations are simulated to occur in the high latitude regions in the Northern Hemisphere (NH) (Fig. 4(a) and Fig. 4(b)). Simulated HNO_3 concentrations at 100 hPa are low over the region of 40−100°E and 10−30°N, which is part of the anticyclone region defined in Fig. 1. Figure 4(c) shows the latitude-altitude cross section of simulated seasonal mean HNO_3 mixing ratios averaged over 70−105°E. In boreal summer, the highest HNO_3 mixing ratios are simulated to occur at 30 hPa over the Polar Regions in both hemispheres. Over high latitudes, HNO_3 concentrations in the Southern Hemisphere (SH) are simulated to be higher than those in the NH.

To evaluate the simulated HNO_3, Figures 4(d)-4(f) show HNO_3 concentrations in the UTLS from MLS that are averaged over June-August of 2005. At 200 and 100 hPa altitudes, the observed HNO_3 mixing ratios are high in the high latitudes in the NH, which are captured by the GEOS-Chem model. The observed HNO_3 at 100 hPa exhibits low values of less than 400 pptv over

299 30–100°E and 10–30°N in the Asian monsoon anticyclone region (Fig. 4(e)). At

300 100 hPa, the observed HNO_3 mixing ratio averaged over the TP/SASM region

301 (70–105°E, 10–40°N) is 301.3 pptv, which is lower than the simulated value of

302 349.1 pptv. The difference between the simulated and observed HNO_3 mixing

303 ratio lies within the confidence range of ±500–1000 pptv of the MLS

304 instruments (Livesey et al., 2011). Considering all the grid cells with MLS

305 HNO_3 data available, the simulated seasonal mean HNO_3 concentrations show

306 normalized mean bias (NMB) of +15.9% at 100 hPa over the TP/SASM region

307 in summer of year 2005. The observed pattern of the HNO_3 vertical distribution

308 (Fig. 4(f)) is also captured by the GEOS-Chem model (Fig. 4(c)). The

309 distributions of HNO_3 in the UTLS are associated with the Brewer-Dobson (BD)

310 circulation proposed by Brewer (1949) and Dobson (1956), traveling upwards

311 across the tropopause to the stratosphere at the equator and downwards to

312 the troposphere near the Polar region.

313 **3.2 O_3**

314 Figure 3(b) shows the global distribution of simulated summertime

315 surface-layer O_3 concentrations. Simulated O_3 concentrations are in a range of

316 40–70 ppbv over Europe, North America, China, and the biomass burning

317 region of South Africa. Our model results agree closely with the simulated

318 distributions and magnitudes reported in Mickley et al. (1999), Collins et al.,

319 (2000), Liao et al. (2003), Wu et al., (2008), Zeng et al. (2008), and Fadnavis et

320 al. (2014). Fadnavis et al. (2014) also presented aircraft measurements over

321 India in September of 2010 during the Cloud Aerosol Interaction and

322 Precipitation Enhancement Experiment (CAIPEEX). Our simulated O_3

323 concentrations of 30–40 ppbv over India agree with the CAIPEEX

324   measurements.

325   Figures 5(a)-5(b) show the simulated O_3 concentrations in the UTLS

326   averaged over June-August of 2005. The distributions of O_3 concentrations in

327   the UTLS are similar to those of HNO_3, with elevated values in the high

328   latitudes of the NH. Relatively low O_3 mixing ratios of less than 200 ppbv are

329   simulated at 100 hPa over 10–30°N, 20–110°E, within the anticyclone region

330   defined in Fig. 1. Our simulated distributions and magnitudes of O_3 agree with

331   those reported in Bian et al. (2011b), which examined the summertime

332   distributions of O_3 in the UTLS during 2005–2009 by using the MLS version 2.2

333   level 2 products (Livesey et al., 2008). Because the background O_3

334   concentrations are generally high in the UTLS and the stratosphere, the low O_3

335   concentrations in the UTLS over the TP/SASM region are caused by the deep

336   convection that transports O_3-poor air upward (Fu et al., 2006; Randel and

337   Park, 2006; Park et al., 2007; Bian et al., 2011b). Figure 5(c) displays the

338   latitude-altitude cross section of seasonal mean O_3 mixing ratios averaged

339   over 70–105°E. As a result of the BD circulation, O_3 concentrations in the

340   UTLS are lower over the tropics than in the Polar Regions, even though the

341   maximum O_3 concentrations are located around 10 hPa over the tropics

342   (Brewer, 1949). Our simulated O_3 concentrations in the UTLS agree well with

343   the measurements from MLS (Fig. 5(d)-5(f)). At 100 hPa, simulated and MLS

344   observed O_3 mixing ratios averaged over the TP/SASM region (70–105°E,

345   10–40°N) are 190.6 and 145.1 ppbv, respectively. Compared to MLS

346   observations, simulated O_3 concentrations at 100 hPa have a NMB of +31.4%

347   over the TP/SASM region in summer of 2005. Our simulated global STE of O_3

348   is 420 Tg yr^{-1}, which is within the range reported in previous studies (475±120

349 Tg yr^{-1} in McLinden et al. (2000), 420 Tg yr^{-1} in Škerlak et al. (2014), 556±154

350 Tg yr^{-1} in Stevenson et al. (2006), and 550±140 Tg yr^{-1} in Solomon et al.

351 (2007)).

352 In addition to the comparisons against MLS products, the simulated O$_3$

353 profiles are compared with balloon-borne sonde measurements in Fig. 6. The

354 measurements were carried out at Kunming (KM, 102.7°E, 25.0°N) in August

355 of 2009 and 2012, and at Lhasa (LH, 91.1°E, 29.7°N) in August of 2010 and

356 2013. The uncertainties of the observed O$_3$ mixing ratios were estimated to be

357 within 5–10% (Bian et al. 2012). The comparisons with multi-year observations

358 show that the model can reproduce the vertical distributions of O$_3$ in Kunming

359 and Lhasa. At 100 hPa, the simulated monthly mean O$_3$ mixing ratio in KM is

360 112.6 ppbv, and the observed value is 124.2 ppbv in 2009 and 113.5 ppbv in

361 2012. In LH, the simulated monthly O$_3$ mixing ratio at 100 hPa is 152.6 ppbv,

362 and the observed O$_3$ mixing ratio at that altitude is 142.4 ppbv in 2010 and

363 167.9 ppbv in 2013. The magnitudes of O$_3$ mixing ratios from these

364 balloon-borne sonde measurements support those from MLS; O$_3$ mixing ratios

365 in the UTLS are less than 200 ppbv over the TP/SASM region.

366

367 **4 Simulated aerosols and model evaluation**

368 **4.1 Simulated aerosols**

369 Figure 7 (a) shows the simulated surface-layer concentrations of SO_4^{2-}, NO_3^-,

370 NH_4^+, OC, BC, and PM$_{2.5}$ (the sum of the mass of SO_4^{2-}, NO_3^-, NH_4^+, BC, and

371 OC aerosols) averaged over June-August of year 2005. As expected,

372 simulated aerosol concentrations are high over polluted regions such as India

373 and eastern China as a result of the high anthropogenic emissions of aerosol

374 precursors and aerosols (Streets et al., 2003; Huang et al., 2012). Over the

375 TP/SASM region (70–105°E, 10–40°N), the average concentrations of SO_4^{2-},

376 NO_3^-, NH_4^+, BC, and OC are 1.70, 0.94, 0.85, 0.30, and 0.94 µg m^{-3},

377 respectively. NO_3^- is simulated to be of secondary importance at the surface

378 over the region of our interest. The simulated distributions and magnitudes of

379 these aerosol species are similar to those reported in Wang et al. (2013) and

380 Mu and Liao (2014).

381 Figures 7(b) and 7(c) also show the simulated concentrations of SO_4^{2-},

382 NO_3^-, NH_4^+, OC, BC, and PM$_{2.5}$ in the UTLS. Elevated concentrations of SO_4^{2-},

383 NO_3^-, NH_4^+, OC, BC and PM$_{2.5}$ are simulated over the TP and Plateau south

384 slope at 200 hPa altitude, and extend from eastern Mediterranean to western

385 China at 100 hPa. The simulated enhanced concentrations of SO_4^{2-}, OC, and

386 BC at 100 hPa over the anticyclone region (20–120°E, 10–40°N) agree with

387 previous observational and modeling studies (Lelieveld et al., 2001; Li et al.,

388 2005; Fadnavis et al., 2013). Li et al. (2005) reported elevated CO

389 concentrations in the upper troposphere over the TP, on the basis of both MLS

390 measurements and the GEOS-Chem simulation for September 2004.

391 Fadnavis et al. (2013) also simulated maximum concentrations of SO_4^{2-}, OC,

392 BC, and mineral dust aerosols in the UTLS during the Asian summer monsoon

393 season owing to convective uplifting of the boundary layer pollutants. With

394 NO_3^- aerosol accounted for in our simulation, NO_3^- is simulated to be the most

395 dominant aerosol species in the UTLS over the TP/SASM region, followed

396 by SO_4^{2-}, NH_4^+, OC, and BC. At 100 hPa, the averaged concentrations of SO_4^{2-},

397 NO_3^-, NH_4^+, OC, and BC over the TP/SASM region (70–105°E, 10–40°N)

398 region are 0.026, 0.069, 0.014, 0.011, and 0.002 µg m^{-3}, respectively.

4.2 Comparisons of simulated aerosol concentrations with in-situ observations

The simulated aerosol concentrations in East Asia in the GEOS-Chem model have been evaluated in previous studies (L. Zhang et al., 2010; Fu et al., 2012; Jeong and Park, 2013; Jiang et al., 2013; Wang et al., 2013; Lou et al., 2014). Here we are focused on the evaluation of aerosols in the South Asian monsoon region. For lack of publicly accessible in situ measurements of summertime aerosols in South Asia monsoon area, we compiled monthly or seasonal mean measured concentrations of each aerosol species based on measurements reported in the literature (see Table S1 in the Supplementary Material). These measurements were carried out over years of 1992−2010. The locations of sites with measurements available are shown in Fig. 8(a). Most sites are located in the upwind directions of the TP, with pollutants that can be transported to the UTLS during the South Asian summer monsoon season. The observed PM_{10} concentrations listed in Table S1 are multiplied by 0.6 to convert to $PM_{2.5}$ for model evaluation, following the suggestions in Zhang et al. (2002) and Chatterjee et al. (2010).

Figures 8(b)−8(f) show the scatterplots of simulated versus observed seasonal mean aerosol concentrations. Compared with measurements, simulated SO_4^{2-}, NO_3^-, NH_4^+, OC and BC have NMBs of −17.0%, +38.8%, +42.0%, −69.7% and −41.0%, respectively, as the concentrations of all seasons are considered. The correlations between model results and observations have R values of 0.49−0.85 for all aerosol species, indicating that the model is capable of capturing the spatial distributions and seasonal variations of each aerosol species in the South Asian monsoon region despite

the biases in concentrations. If we consider simulated and measured concentrations for JJA alone, the simulated concentrations of SO_4^{2-}, NO_3^-, NH_4^+, OC and BC exhibit seasonal NMBs of −14.7%, +51.5%, +74.9%, −57.2% and −32.2%, respectively, and the values of R are in the range of 0.24−0.85. Note that the measurements of NO_3^- and NH_4^+ are quite limited in terms of the number of samples, and the discrepancies between model results and measurements may also arise from the mismatch of the model year 2005 with the years of 1992−2010 with observations available.

4.3 Comparisons of simulated aerosol extinction coefficients with SAGE II datasets

Satellite datasets from the Stratospheric Aerosol and Gas Experiment II (SAGE II, https://eosweb.larc.nasa.gov/project/sage2/sage2_v620_table) are used to evaluate the simulated aerosol extinction in the UTLS. The SAGE II instrument was launched in October 1984 aboard the Earth Radiation Budget Satellite (ERBS) and terminated on 8 September 2005 (McCormick et al. 1987; Chu et al. 1989). The datasets used here are aerosol extinction coefficients at 525 nm from the version 6.20 SAGE retrievals, covering from 0.5 to 40 km with a vertical resolution of 0.5 km. Many validation studies have been conducted on the SAGE II aerosol data (Russell and McCormick, 1989; Oberbeck et al., 1989; Wang et al., 1989), which indicated that extinction coefficients have uncertainties of 20−30%. The extinction coefficients of aerosols in the GEOS-Chem model are calculated using aerosol mass concentration, extinction efficiency, effective radius, particle mass density, and the assumed aerosol size distribution (Drury et al., 2010). The hygroscopic growth of each aerosol species with relative humidity is accounted for, using the hygroscopic

growth factors listed in Martin et al. (2003).

Figure 9(a) presents the simulated monthly mean distribution of aerosol extinction coefficients at 100 hPa for July of 2005. At 100 hPa, the simulated aerosol extinction coefficients are relatively high over the anticyclone region, where anthropogenic aerosol species (Fig. 7) and natural aerosols such as mineral dust and sea salt contribute to aerosol extinction coefficients in summer. Note that the contributions of sulfate, nitrate, ammonium, OC, sea salt, and mineral dust are all considered when we calculate aerosol extinction coefficients. Aerosol extinction coefficients are simulated to be $1.2-2\times10^{-3}$ km^{-1} at 100 hPa over the Asian continent and Indian Ocean (20°S$-$30°N, 30°$-$105°E). These values agree closely with aerosol extinction coefficients measured at Naqu during August of 2011 for the same altitude, the maximum of which was 2.4×10^{-3} km^{-1} (He et al., 2014). Vernier et al. (2011) also identified this Asian aerosol layer with high SR at 100 hPa by observations of CALIPSO for JJA of 2006$-$2008.

Figure 9(b) displays the monthly mean vertical profiles of aerosol extinction coefficients averaged over the Asian monsoon anticyclone region (20$-$120°E 10$-$40°N) (Fig. 1) for July of 2005. The SAGE II datasets are available for July only in 2005. The profiles from SAGE II and the GEOS-Chem simulation are all shown. Accounting for all aerosol species, the GEOS-Chem model reproduces well the aerosol extinction coefficients above 10 km, but the discrepancies are rather large in altitudes less than 10 km. Note that the uncertainties in satellite datasets increase as the altitude decreases (Vanhellemont et al., 2008；Kulkarni and Ramachandran, 2015), and the missing data in the lower troposphere along the satellite trajectories over the region of our interest also

474   contribute to the discrepancies

475   Comparisons of profiles of aerosol extinction coefficients with and without

476   nitrate aerosol indicate that the profiles show small differences in altitudes less

477   than 6 km but large discrepancies from 6 km to the tropopause. With nitrate

478   aerosol accounted for, the simulated aerosol extinction coefficients agree

479   closely with SAGE II datasets in the UTLS (averaged over 14−16 km, the

480   simulated value is 8.6×10^{-4} km^{-1} while the observed value is 8.0×10^{-4} km^{-1}).

481   Without nitrate aerosol, the simulated aerosol extinction coefficient at 14−16

482   km altitude is 1.5×10^{-4} km^{-1}, which underestimates the aerosol extinction

483   coefficient by 82.6% compared to that calculated with all the aerosol species.

484   These comparisons of extinction coefficients with and without nitrate aerosol

485   suggest that nitrate aerosol plays an important role in aerosol extinction in the

486   UTLS over the region of our interest.

487

488   **5 Contribution of nitrate to aerosol concentrations in the UTLS**

489   Since nitrate aerosol is simulated to be the most abundant aerosol species in

490   the UTLS over the TP/SASM region, we analyze the contribution of nitrate to

491    $PM_{2.5}$ concentration (C_{NIT}=nitrate concentration/$PM_{2.5}$ concentration) in this

492   section. Figure 10 shows the simulated seasonal mean distributions of C_{NIT} for

493   June-August of year 2005. At the surface layer (Fig. 10(a)), simulated high C_{NIT}

494   values are located over the areas with high nitrate concentrations (India and

495   eastern China) as well as the oceans where NO_3^- also forms on sea salt and

496   mineral dust particles (Arimoto et al., 1996; Nakamura et al., 2005; George and

497   Nair, 2008). Over the TP/SASM region, the C_{NIT} values in JJA are 5–35% at the

498   surface, 25–50% at 200 hPa (Fig. 10(b)), and could exceed 60% at 100 hPa

499 (Fig. 10(c)). The latitude-altitude cross section of C_{NIT} (Fig. 10(d)) shows that

500 C_{NIT} over 20–40°N increases with altitude and reaches maximum values

501 around the extratropical tropopause.

502 Table 2 lists the mean concentrations of SO_4^{2-}, NO_3^-, NH_4^+, BC and OC, and

503 their contributions to $PM_{2.5}$ during summertime of 2005 over the TP/SASM, TP,

504 and SASM regions. Over the TP/SASM region, SO_4^{2-}, NO_3^-, NH_4^+, BC and OC

505 are simulated to contribute 35.9%, 19.8%, 18.1%, 6.4%, and 19.8%,

506 respectively, to $PM_{2.5}$ mass concentration at the surface layer. The

507 contributions increase significantly in the UTLS. The largest C_{NIT} is simulated

508 in the SASM region at 100 hPa, where NO_3^- accounts for 60.5% of $PM_{2.5}$ mass

509 concentration. The high C_{NIT} values indicate that NO_3^- plays an important role

510 in the aerosol layer in the UTLS over the TP/SASM region.

511

512 **6 Mechanisms for high nitrate concentrations in the UTLS**

513 **6.1 Upward transport of nitrate from the lower troposphere**

514 The intense convective transport of chemical species into the UTLS over the

515 TP/SASM region during summertime has been widely discussed in previous

516 studies (Randel et al., 2010; Bian et al., 2011a; Fadnavis et al., 2013, 2014;

517 Qie et al., 2014; He et al., 2014). Since nitrate aerosol is simulated to be of

518 secondary abundant aerosol species in the surface layer over the TP/SASM

519 region (Fig. 7), the vertical mass transport through the deep convection in this

520 region contributes to the accumulation of NO_3^- in the UTLS. Figure 11 shows

521 the latitude-altitude cross sections of simulated concentrations of SO_4^{2-} and

522 NO_3^- averaged over 70–105°E in June-August of 2005, together with the

523 wind vectors obtained from the European Centre for Medium-Range Weather

Forecasts (ECMWF) ERA-Interim Reanalysis data. Note that the assimilated GEOS-5 meteorological fields do not have vertical winds (http://wiki.seas.harvard.edu/geos-chem/index.php/List_of_GEOS-5_met_fields), so we use the ECMWF reanalysis wind fields to do the analysis here. High values of aerosol concentrations are found on the south slope of the Himalayas, where the deep convection exists. Although both SO_4^{2-} and NO_3^- are transported upward to the extratropical tropopause, the details of the vertical distributions are different. At altitudes higher than 8 km, the concentrations of NO_3^- do not decrease with altitude as quickly as those of SO_4^{2-}, and the concentrations of NO_3^- over 10–40°N are higher than those of SO_4^{2-}.

The chemical mechanisms for the formation of SO_4^{2-}, NO_3^-, and NH_4^+ aerosols in the GEOS-Chem model were described in R. J. Park et al. (2004), which are comprehensive and have been used extensively in previous studies to simulate these three aerosol species (R. J. Park et al., 2004; Pye et al., 2009; L. Zhang et al., 2010; Zhu et al., 2012; Jiang et al., 2013; Lou et al., 2014). Sulfate aerosol forms from gas-phase oxidation of SO_2 by OH and from in-cloud oxidation of SO_2 by O_3 and H_2O_2. Nitrate forms from the partitioning of HNO_3 between gas and aerosol phases, which is calculated by the ISORROPIA II thermodynamic equilibrium module (Fountoukis and Nenes, 2007) in the GEOS-Chem model. Major reactions for the production and loss of HNO_3 were listed in Liao and Seinfeld (2005). HNO_3 is produced by the reaction of NO with OH during daytime and by hydrolysis of N_2O_5 on aerosol surfaces at night. The chemical mechanisms for SO_4^{2-} and NO_3^- have different sensitivity to meteorological conditions. During the vertical transport,

549 temperature decreases, which reduces the gas-phase oxidation of SO_2 (Yao et

550 al., 2002; Seinfeld and Pandis 2006; X. Y. Zhang et al., 2012) but promotes the

551 formation of NO_3^- by shifting gas-particle equilibria (Dawson et al., 2007; Liao

552 et al., 2009). Therefore the different chemical mechanisms for SO_4^{2-} and NO_3^-

553 formation contribute to the differences in their vertical distributions.

6.2 The gas-to-aerosol conversion of HNO_3 to form nitrate

As mentioned above, the formation of gas-phase HNO_3 and the partitioning of

HNO_3 between gas and aerosol phases are the two major chemical processes

that influence NO_3^- concentrations. We have evaluated the ability of the

GEOS-Chem model to simulate gas-phase HNO_3 in Section 3.1 (by

comparisons of our model results with MLS observations and concentrations

from previous modeling studies), so we quantify here NO_3^- formation from

gas-to-aerosol conversion of HNO_3 based on the ISORROPIA II

thermodynamic equilibrium module (Fountoukis and Nenes, 2007). The

gas-to-aerosol conversion of HNO_3 to form NO_3^- is very sensitive to relative

humidity (RH) and temperature (Fountoukis and Nenes 2007; Dawson et al.,

2007). Low temperature and high RH are favorable for NO_3^- formation. Figure

12 shows the seasonal mean horizontal distributions of RH and temperature at

100 hPa and the latitude-altitude cross sections of these two parameters

averaged over 70−105°E. RH exhibits high values in the TP/SASM region,

which are consistent with the high H_2O mixing ratios in this area reported in

Gettelman et al. (2004), M. Park et al. (2004), and Fu et al. (2006). At 100 hPa,

the locations with high RH of exceeding 45% correspond well with those with

high C_{NIT} values (Fig. 10(c)). The latitude-altitude cross section of RH (Fig.

12(c)) shows that RH has high values over the places with intense upward

transport (Fig. 11). For temperature, as Fig. 12(b) and 12(d) show, summertime temperatures are cold (190–200 K) at 100 hPa in the TP/SASM region, consistent with the distribution and magnitude reported for August, 2011, in He et al. (2014) on the basis of the NCEP Reanalysis data. The low temperatures over the TP/SASM region are associated with the adiabatic expansion of ascending air mass of the deep convections (Yanai et al., 1992; Park et al., 2007; He et al., 2014).

Because of the favorable conditions of RH and temperature, the gas-to-aerosol conversion of HNO_3 to form nitrate can occur during the upward transport and in the UTLS. Figure 13 shows the mass budget for nitrate aerosol within the selected box of (70–105°E, 10–40°N, 8–16 km) to see the role of nitrate formation over the TP/SASM region. The horizontal mass fluxes have a net negative value of 0.10 Tg season^{-1}, reducing nitrate aerosol in the selected box. The vertical transport and the gas-to-aerosol conversion of HNO_3 increase nitrate mass in the selected box, with values of 0.09 Tg season^{-1} and 0.11 Tg season^{-1}, respectively, indicating that the gas-to-aerosol conversion plays an important role in the enhancement of nitrate in the UTLS over the TP/SASM region. Although relatively high RH exists near the tropopause of the TP/SASM region, the air near the tropopause is still dryer compared to that in the lower altitudes. Model results show that the gas-to-aerosol partition of HNO_3 decreases with altitude over 8–16 km, indicating that the gas to aerosol conversion contributes to nitrate accumulation in the UTLS mainly during the process of upward transport.

Previous studies have also reported that nitric acid trihydrates (NAT, $HNO_3 \cdot (H_2O)_3$) could form in the polar and tropical stratosphere at low

44

temperatures through two mechanisms: (1) the homogeneous nucleation out of supercooled ternary solutions, and (2) the heterogeneous formation on ice particles (Hofmann et al., 1989; Carslaw et al., 1998; Voigt et al., 2000; Popp et al., 2006; Kirner et al., 2011). A typical NAT condensation temperature is approximate 193 K (Kirner et al., 2011). As shown in Fig. 12, the temperatures around 100 hPa over the TP/SASM region are in the range of 190–200 K, which are low enough to produce some NAT particles. However, balloon-borne measurements of depolarization ratio and backscattering ratio of aerosols at Lhasa during August-October of 1999 by Kim et al. (2003) and Tobo et al. (2007) suggested that coarse and aspherical particles such as NAT are scarce in the UTLS of the TP/SASM.

7 Impacts of uncertainties in surface-layer aerosol concentrations on simulated nitrate in the UTLS

Since simulated SO_4^{2-}, NO_3^- and NH_4^+ concentrations have, respectively, NMBs of −17.0%, +38.8%, and +42.0% on an annual mean basis and of −14.7%, +51.5%, and +74.9% in summer (Section 4.2), we perform four sensitivity simulations to examine the impacts of uncertainties in surface-layer aerosol concentrations on simulated nitrate in the UTLS. In the first three cases, anthropogenic emissions of NO_x, NH_3, and SO_2 in Asia are changed by −50%, −50%, and +20%, respectively, relative to those in our standard simulation. In the last case, anthropogenic emissions of all these three species are changed simultaneously, with NO_x reduced by 50%, NH_3 reduced by 50%, and SO_2 increased by 20% in Asia relative to the standard case. The purpose of these sensitivity studies is to reduce NMBs of simulated surface-layer

concentrations of SO_4^{2-}, NO_3^- and NH_4^+ and see whether NO_3^- is still the most dominant aerosol species in the UTLS. Model results from these sensitivity studies for summer of 2005 are presented in Table 3.

As anthropogenic emissions of SO_2 in Asia are increased by 20%, the NMB of simulated surface-layer SO_4^{2-} concentrations is −4.4%, which is an improvement compared to the NMB of −14.7% in the standard simulation. However, the increases in SO_2 emissions lead to larger NMBs of surface-layer NO_3^- and NH_4^+ because of the increased formation of ammonium sulfate or ammonium bisulfate. The percentage contributions of SO_4^{2-} to total aerosol mass in the UTLS increase slightly by 2.7% at 200 hPa and by 1.6% at 100 hPa, and nitrate in the UTLS also shows small sensitivity to the change in SO_2 emissions.

With anthropogenic emissions of NO_x in Asia reduced by 50%, the NMB of simulated surface-layer NO_3^- concentrations changes from +51.5% in the standard simulation to −11.7% in this sensitivity run. The contribution of each of SO_4^{2-}, NO_3^- and NH_4^+ aerosols to total aerosol mass in the UTLS is not sensitive to this reduction in NO_x emissions at the surface; the percentage contribution obtained from this sensitivity run is very close to the value obtained in the standard simulation (Table 3). Similarly, in the sensitivity study with NH_3 emissions reduced by 50% in Asia, simulated surface-layer concentrations of NO_3^- and NH_4^+ are improved in terms of the values of NMBs, but the improvement in simulated aerosol concentrations at the surface-layer does not influence our conclusion of high nitrate aerosol concentration in the UTLS.

In the sensitivity study with emissions of NO_x, NH_3, and SO_2 in Asia

649 changed simultaneously, simulated surface-layer concentrations of SO_4^{2-}, NO_3^-

650 and NH_4^+ have NMBs of −8.3%, −27.0% and +55.4%, respectively, which are

651 all improved compared to those in the standard simulation. Even though nitrate

652 aerosol is now underestimated at the surface, it still accounts for 53.3% of the

653 $PM_{2.5}$ concentration at 100 hPa over the TP/SASM region in summer.

654 It should be noted that the concentrations of OC and BC are also

655 underestimated, with NMBs of −57.2% and −32.2%, respectively, in summer

656 (Section 4.2). We have done a simple calculation with the concentrations of

657 OC and BC in the UTLS multiplied by 2.3 and 1.5, respectively, and nitrate is

658 still the most dominant aerosol species in summertime in the UTLS over the

659 TP/SASM region (not shown in Table 3). Therefore the uncertainties in surface

660 aerosol concentrations do not compromise the conclusion of this study.

661

662 **8 Conclusions**

663 In this work we simulate nitrate aerosol and its contribution to aerosol

664 concentrations in the UTLS over the TP/SASM region (70–105°E, 10–40°N)

665 for summertime of year 2005, using the global chemical transport model

666 GEOS-Chem driven by the assimilated meteorological fields.

667 Simulated HNO_3 and O_3 are evaluated to show the model's ability to

668 simulate the NOx-O_3-HNO_3 cycle over the studied region. In the UTLS, both

669 the horizontal and vertical distributions of simulated HNO_3 and O_3 agree well

670 with the MLS observations. At 100 hPa, simulated seasonal mean HNO_3 and

671 O_3 mixing ratios show NMBs of +15.9% and +31.4%, respectively, over the

672 TP/SASM region (70–105°E, 10–40°N) in summer of year 2005, and the model

673 biases lie within the confidence range of the MLS instruments. Both simulated

674 and observed O_3 concentrations show relatively low values of less than 200

675 ppbv at 100 hPa over the TP/SASM region.

676   Averaged over the TP/SASM region, the surface-layer concentrations of

677 SO_4^{2-}, NO_3^-, NH_4^+, BC, and OC are simulated to be 1.70, 0.94, 0.85, 0.30, and

678 0.94 μg m^{-3}, respectively. ==Nitrate aerosol is simulated to be of secondary==

679 ==importance near the surface over the region of our interest.== Comparisons of

680 simulated aerosol concentrations with ground-based observations show that

681 simulated summertime concentrations of SO_4^{2-}, NO_3^-, NH_4^+, OC and BC have

682 NMB of −14.7%, +51.5%, +74.9%, −57.2% and −32.2%, respectively. Note that

683 the measurements of NO_3^- and NH_4^+ are quite limited in terms of the number

684 of samples.

685   Model results show elevated concentrations of SO_4^{2-}, NO_3^-, NH_4^+, OC, BC

686 and PM$_{2.5}$ in the UTLS over the TP/SASM region throughout the summer. NO_3^-

687 is simulated to be the most dominant aerosol species in the UTLS of the

688 TP/SASM region. Accounting for NO_3^- aerosol, the GEOS-Chem model

689 reproduces well the magnitude of aerosol extinctions above 10 km, as model

690 results are compared with the SAGE II measurements. ==The discrepancies==

691 ==between the simulated and observed aerosol extinction coefficient are within 8%==

692 ==in the UTLS (averaged over 14–16 km).== Simulated vertical profiles of aerosol

693 extinction coefficients with and without nitrate aerosol show large

694 discrepancies from 6 km to tropopause, indicating the important role of nitrate

695 in aerosol layer in the UTLS over the TP/SASM region.

696   The contribution of NO_3^- to aerosols in the TP/SASM region is quantified

697 by C$_{NIT}$ (the ratio of nitrate concentration to PM$_{2.5}$ concentration). Over the

698 TP/SASM region, the C$_{NIT}$ values in summer are 5–35% at the surface, 25–

50% at 200 hPa, and could exceed 60% at 100 hPa. The mechanisms for the accumulation of nitrate in the UTLS over the TP/SASM region include vertical transport and the gas-to-aerosol conversion of HNO_3 to form nitrate. Such gas-to-aerosol conversion occurs during the upward transport and in the UTLS. The high relative humidity and low temperature associated with the deep convection over the TP/SASM region are favorable for nitrate formation.

Results from the present study indicate that nitrate is an important aerosol species in the UTLS over the ASM/TP region. Considering the scarce measurements of nitrate in the UTLS and the model uncertainties, more observational and modeling studies are needed to further explore the aerosol composition in the Asian tropopause aerosol layer. Further simulations of nitrate aerosol in the UTLS also need to account for NAT formation at low temperatures (Kirner et al., 2011) and the roles of natural aerosols, including the transport of mineral dust and sea salt to the UTLS as well as nitrate formation on these natural particles (Ma et al., 2003).

References

Adhikary, B., Carmichael, G. R., Tang, Y., Leung, L. R., Qian, Y., Schauer, J. J., Stone, E. A., Ramanathan, V., and Ramana, M. V.: Characterization of the seasonal cycle of south Asian aerosols: A regional-scale modeling analysis, J. Geophys. Res., 112, D22S22, doi:10.1029/2006JD008143, 2007.

Alexander, B., Park, R. J., Jacob, D. J., Li, Q., Yantosca, R. M., Savarino, J., Lee, C., and Thiemens, M.: Sulfate formation in sea-salt aerosols: Constraints from oxygen isotopes, J. Geophys. Res., 110, D10307, doi:10.1029/2004JD005659, 2005.

Arimoto, R., Duce, R., Savoie, D., Prospero, J., Talbot, R., Cullen, J., Tomza, U., Lewis, N., and Ray, B.: Relationships among aerosol constituents from Asia and the North Pacific during PEM–West A, J. Geophys. Res., 101, 2011–2023, 1996.

Babu, S. S. and Moorthy, K. K.: Aerosol black carbon over a tropical coastal station in India, Geophys. Res. Lett., 29, 2098, doi:10.1029/2002GL015662, 2002.

Bano, T., Singh, S., Gupta, N., Soni, K., Tanwar, R., Nath, S., Arya, B., and Gera, B.: Variation in aerosol black carbon concentration and its emission estimates at the mega-city Delhi, Int. J. Remote Sens., 32, 6749–6764, 2011.

Bian, J., Yan, R., and Chen, H.: Tropospheric Pollutant Transport to the Stratosphere by Asian Summer Monsoon, Chinese Journal of Atmospheric Sciences, 35, 897–902, 2011a.

Bian, J., Yan, R., Chen, H., Lü, D., and MASSIE, S. T.: Formation of the Summertime Ozone Valley over the Tibetan Plateau: The Asian Summer Monsoon and Air Column Variations, Adv. Atmos. Sci., 28, 1318–1325, 2011b.

Bian, J., Pan, L. L., Paulik, L., Vömel, H., Chen, H., and Lü, D.: In situ water vapor and ozone measurements in Lhasa and Kunming during the Asian summer monsoon, Geophys. Res. Lett., 39, L19808, doi:10.1029/2012GL052996, 2012.

Bourgeois, Q., Bey, I., and Stier, P.: A permanent aerosol layer at the tropical tropopause layer driven by the intertropical convergence zone, Atmos. Chem. Phys. Discuss., 12, 2863–2889, 2012.

Bouwman, A., Lee, D., Asman, W., Dentener, F., Van Der Hoek, K., and Olivier, J.: A global high-resolution emission inventory for ammonia, Global Biogeochem. Cy., 11, 561-587, 1997.

Brewer, A. W.: Evidence for a world circulation provided by the measurements of helium and water vapour distribution in the stratosphere, Q. J. Roy. Meteor. Soc., 75, 351-363, 1949.

Carrico, C. M., Bergin, M. H., Shrestha, A. B., Dibb, J. E., Gomes, L., and Harris, J. M.: The importance of carbon and mineral dust to seasonal aerosol properties in the Nepal Himalaya, Atmos. Environ., 37, 2811–2824, 2003.

Carslaw, K., Wirth, M., Tsias, A., Luo, B., Dörnbrack, A., Leutbecher, M., Volkert, H., Renger, W., Bacmeister, J., and Peter, T.: Particle microphysics and chemistry in remotely observed mountain polar stratospheric clouds, J. Geophys. Res., 103, 5785–5796, 1998.

Chatterjee, A., Adak, A., Singh, A. K., Srivastava, M. K., Ghosh, S. K., Tiwari, S., Devara, P. C., and Raha, S.: Aerosol chemistry over a high altitude

station at northeastern Himalayas, India, PloS one, 5, e11122, doi:10.1371/journal.pone.0011122, 2010.

Chatterjee, A., Ghosh, S. K., Adak, A., Singh, A. K., Devara, P. C., and Raha, S.: Effect of Dust and Anthropogenic Aerosols on Columnar Aerosol Optical Properties over Darjeeling (2200 m asl), Eastern Himalayas, India, PloS one, 7, e40286, doi:10.1371/journal.pone.0040286, 2012.

Chen, H., Bian, J., and Lü, D.: Advances and prospects in the study of stratosphere-troposphere exchange, Chinese J. Atmos. Sci., 30, 813–820, doi:1006-9895(2006)30:5<813:SDLCXP>2.0.TX;2-A, 2006.

Chowdhury, Z., Zheng, M., Schauer, J. J., Sheesley, R. J., Salmon, L. G., Cass, G. R., and Russell, A. G.: Speciation of ambient fine organic carbon particles and source apportionment of $PM_{2.5}$ in Indian cities, J. Geophys. Res., 112, D15303, doi:10.1029/2007JD008386, 2007.

Chu, W., McCormick, M., Lenoble, J., Brogniez, C., and Pruvost, P.: SAGE II inversion algorithm, J. Geophys. Res., 94, 8339–8351, 1989.

Collins, W. J., Stevenson, D. S., Johnson, C. E., and Derwent, R. G.: The European regional ozone distribution and its links with the global scale for the years 1992 and 2015, Atmos. Environ., 34, 255–267, 2000.

Considine, D. B., Rosenfield, J. E., and Fleming, E. L.: An interactive model study of the influence of the Mount Pinatubo aerosol on stratospheric methane and water trends, J. Geophys. Res., 106, 27711-27727, doi:10.1029/2001jd000331, 2001.

Considine, D. B., Logan, J. A., and Olsen, M. A.: Evaluation of near-tropopause ozone distributions in the Global Modeling Initiative combined stratosphere/troposphere model with ozonesonde data, Atmos. Chem. Phys., 8, 2365–2385, 2008.

Datta, A., Sharma, S., Harit, R., Kumar, V., Mandal, T., and Pathak, H.: Ammonia emission from subtropical crop land area in India, Asia-Pac. J. Atmos. Sci., 48, 275–281, 2012.

Dawson, J., Adams, P., and Pandis, S.: Sensitivity of $PM_{2.5}$ to climate in the Eastern US: a modeling case study, Atmos. Chem. and phys., 7, 4295–4309, 2007.

Decesari, S., Facchini, M., Carbone, C., Giulianelli, L., Rinaldi, M., Finessi, E., Fuzzi, S., Marinoni, A., Cristofanelli, P., and Duchi, R.: Chemical composition of PM_{10} and PM_1 at the highaltitude Himalayan station Nepal Climate Observatory-Pyramid (NCO-P)(5079 m asl), Atmos. Chem. Phys, 10, 4583–4596, 2010.

Dobson, G. M. B.: Origin and distribution of the polyatomic molecules in the atmosphere, Proceedings of the Royal Society of London. Series A, Mathematical and Physical Sciences, 187–193, 1956.

Drury, E., Jacob, D. J., Spurr, R. J., Wang, J., Shinozuka, Y., Anderson, B. E., Clarke, A. D., Dibb, J., McNaughton, C., and Weber, R.: Synthesis of satellite (MODIS), aircraft (ICARTT), and surface (IMPROVE, EPA–AQS, AERONET) aerosol observations over eastern North America to improve MODIS aerosol retrievals and constrain surface aerosol concentrations and sources, J. Geophys. Res., 115, D14204, doi:10.1029/2009JD012629, 2010.

Duncan, B., Strahan, S., Yoshida, Y., Steenrod, S., and Livesey, N.: Model study of the cross-tropopause transport of biomass burning pollution, Atmos. Chem. Phys., 7, 3713–3736, 2007.

Dutkiewicz, V. A., Alvi, S., Ghauri, B. M., Choudhary, M. I., and Husain, L.: Black carbon aerosols in urban air in South Asia, Atmos. Environ., 43, 1737–1744, 2009.

Evans, M., and Jacob, D. J.: Impact of new laboratory studies of N_2O_5 hydrolysis on global model budgets of tropospheric nitrogen oxides, ozone, and OH, Geophys. Res. Lett., 32, 10 L09813, doi:10.1029/2005GL022469, 2005.

Fadnavis, S., Semeniuk, K., Pozzoli, L., Schultz, M., Ghude, S., Das, S., and Kakatkar, R.: Transport of aerosols into the UTLS and their impact on the Asian monsoon region as seen in a global model simulation, Atmos. Chem. Phys., 13, 8771–8786, 2013.

Fadnavis, S., Semeniuk, K., Schultz, M., Mahajan, A., Pozzoli, L., Sonbawane, S., and Kiefer, M.: Transport pathways of peroxyacetyl nitrate in the upper troposphere and lower stratosphere from different monsoon systems during the summer monsoon season, Atmos. Chem. Phys. Discuss., 14, 20159–20195, 2014.

Fairlie, T. D., Jacob, D. J., and Park, R. J.: The impact of transpacific transport of mineral dust in the United States, Atmos. Environ., 41, 1251–1266, 2007.

Fisher, J. A., Jacob, D. J., Wang, Q., Bahreini, R., Carouge, C. C., Cubison, M. J., Dibb, J. E., Diehl, T., Jimenez, J. L., and Leibensperger, E. M.: Sources, distribution, and acidity of sulfate–ammonium aerosol in the Arctic in winter–spring, Atmos. Environ., 45, 7301–7318, 2011.

Fountoukis, C., and Nenes, A.: ISORROPIA II: a computationally efficient thermodynamic equilibrium model for K^+–Ca^{2+}–Mg^{2+}–NH_4^+–Na^+–SO_4^{2-}–NO_3^-–Cl^-–H_2O aerosols, Atmos. Chem. Phys., 7, 4639–4659, 2007.

Froyd, K., Murphy, D., Sanford, T., Thomson, D., Wilson, J., Pfister, L., and Lait, L.: Aerosol composition of the tropical upper troposphere, Atmos. Chem. Phys., 9, 4363–4385, 2009.

Fu, R., Hu, Y., Wright, J. S., Jiang, J. H., Dickinson, R. E., Chen, M., Filipiak, M., Read, W. G., Waters, J. W., and Wu, D. L.: Short circuit of water vapor and polluted air to the global stratosphere by convective transport over the Tibetan Plateau, P. Natl. A. Sci., 103, 5664–5669, 2006.

Fu, T. -M., Cao, J., Zhang, X., Lee, S., Zhang, Q., Han, Y., Qu, W., Han, Z., Zhang, R., and Wang, Y.: Carbonaceous aerosols in China: top–down constraints on primary sources and estimation of secondary contribution, Atmos. Chem. Phys., 12, 2725–2746, 2012.

Ganguly, D., Jayaraman, A., and Gadhavi, H.: Physical and optical properties of aerosols over an urban location in western India: Seasonal variabilities, J. Geophys. Res., 111, D24206, doi:10.1029/2006JD007392, 2006.

George, S. K., and Nair, P. R.: Aerosol mass loading over the marine environment of Arabian Sea during ICARB: Sea-salt and non-sea-salt components, J. Earth Syst. Sci., 117, 333–344, 2008.

George, S. K., Nair, P. R., Parameswaran, K., Jacob, S., and Abraham, A.: Seasonal trends in chemical composition of aerosols at a tropical coastal site of India, J. Geophys. Res., 113, D16209, doi:10.1029/2007JD009507, 2008.

Gettelman, A., Kinnison, D. E., Dunkerton, T. J., and Brasseur, G. P.: Impact of monsoon circulations on the upper troposphere and lower stratosphere, J.

874   Geophys. Res., 109, D22101, doi:10.1029/2004JD004878, 2004.

875 Guenther, A., Karl, T., Harley, P., Wiedinmyer, C., Palmer, P., and Geron, C.:
876   Estimates of global terrestrial isoprene emissions using MEGAN (Model of
877   Emissions of Gases and Aerosols from Nature), Atmos. Chem. Phys.
878   Discuss., 6, 107–173, 2006.

879 Hack, J. J.: Parameterization of moist convection in the National Center for
880   Atmospheric Research community climate model (CCM2), J. Geophys.
881   Res., 99, 5551–5568, doi:10.1029/93jd03478, 1994.

882 He, Q., Li, C., Ma, J., Wang, H., Yan, X., Liang, Z., and Qi, G.: Enhancement of
883   aerosols in UTLS over the Tibetan Plateau induced by deep convection
884   during the Asian summer monsoon, Atmos. Chem. Phys. Discuss., 14,
885   3169-3191, 10.5194/acpd–14–3169–2014, 2014.

886 Hegde, P., Sudheer, A., Sarin, M., and Manjunatha, B.: Chemical
887   characteristics of atmospheric aerosols over southwest coast of India,
888   Atmos. Environ., 41, 7751–7766, 2007.

889 Hofmann, D., Rosen, J., Harder, J., and Hereford, J.: Balloon-borne
890   measurements of aerosol, condensation nuclei, and cloud particles in the
891   stratosphere at McMurdo Station, Antarctica, during the spring of 1987, J.
892   Geophys. Res., 94, 11253–11269, doi:10.1029/JD094iD09p11253, 1989.

893 Huang, C., Chen, C. H., Li, L., Cheng, Z., Wang, H. L., Huang, H. Y., Streets, D.
894   G., and Wang, Y. J.: Emission inventory of anthropogenic air pollutants
895   and VOC species in the Yangtze River Delta region, China, Atmos. Chem.
896   Phys., 11, 4105–4120, 2011.

897 Huang, X., Song, Y., Li, M., Li, J., Huo, Q., Cai, X., Zhu, T., Hu, M., and Zhang,
898   H.: A high-resolution ammonia emission inventory in China, Global
899   Biogeochem. Cy., 26, GB1030, doi:10.1029/2011GB004161, 2012.

900 Husain, L., Dutkiewicz, V. A., Khan, A., and Ghauri, B. M.: Characterization of
901   carbonaceous aerosols in urban air, Atmos. Environ., 41, 6872–6883,
902   2007.

903 Jacob, D. J.: Heterogeneous chemistry and tropospheric ozone, Atmos.
904   Environ., 34, 2131-2159, 2000.

905 Jaeglé, L., Quinn, P., Bates, T., Alexander, B., and Lin, J.-T.: Global distribution
906   of sea salt aerosols: new constraints from in situ and remote sensing
907   observations, Atmos. Chem. Phys., 11, 3137–3157, 2011.

908 Jayaraman, A., Gadhavi, H., Ganguly, D., Misra, A., Ramachandran, S., and
909   Rajesh, T.: Spatial variations in aerosol characteristics and regional
910   radiative forcing over India: Measurements and modeling of 2004 road
911   campaign experiment, Atmos. Environ., 40, 6504–6515, 2006.

912 Jeong, J. I., and Park, R. J.: Effects of the meteorological variability on regional
913   air quality in East Asia, Atmos. Environ., 69, 46–55, 2013.

914 Jiang, H., Liao, H., Pye, H., Wu, S., Mickley, L. J., Seinfeld, J. H., and Zhang,
915   X.: Projected effect of 2000-2050 changes in climate and emissions on
916   aerosol levels in China and associated transboundary transport, Atmos.
917   Chem. Phys., 13, 7937–7960, 2013.

918 Kar, J., Bremer, H., Drummond, J. R., Rochon, Y. J., Jones, D., Nichitiu, F., Zou,
919   J., Liu, J., Gille, J. C., and Edwards, D. P.: Evidence of vertical transport of
920   carbon monoxide from Measurements of Pollution in the Troposphere
921   (MOPITT), Geophys. Res. Lett., 31, L23105, doi:10.1029/2004GL021128,
922   2004.

923 Kim, J., Song, C. H., Ghim, Y., Won, J., Yoon, S., Carmichael, G., and Woo, J.

H.: An investigation on NH_3 emissions and particulate $NH_4^+ - NO_3^-$ formation in East Asia, Atmos. Environ., 40, 2139–2150, 2006.

Kim, Y.- S., Shibata, T., Iwasaka, Y., Shi, G., Zhou, X., Tamura, K., and Ohashi, T.: Enhancement of aerosols near the cold tropopause in summer over Tibetan Plateau: lidar and balloonborne measurements in 1999 at Lhasa, Tibet, China, in: Lidar Remote Sensing for Industry and Environment Monitoring III, edited by: Singh U. N., Itabe, T., and Liu, Z., Proceedings of SPIE, Hangzhou, China, 4893, 496–503, 2003.

Kirner, O., Ruhnke, R., Buchholz-Dietsch, J., Jöckel, P., Brühl, C., and Steil, B.: Simulation of polar stratospheric clouds in the chemistry-climate-model EMAC via the submodel PSC, Geoscientific Model Development, 4, 169–182, 2011.

Kulkarni, P., and Ramachandran, S.: Comparison of aerosol extinction between lidar and SAGE II over Gadanki, a tropical station in India, Ann. Geophys., 2015, 351–362,

Kulshrestha, U., Saxena, A., Kumar, N., Kumari, K., and Srivastava, S.: Chemical composition and association of size-differentiated aerosols at a suburban site in a semi-arid tract of India, J. Atmos. Chem., 29, 109–118, 1998.

Latha, K. M., and Badarinath, K.: Seasonal variations of black carbon aerosols and total aerosol mass concentrations over urban environment in India, Atmos. Environ., 39, 4129–4141, 2005.

Lau, K. M., Kim, M. K., and Kim, K. M.: Asian summer monsoon anomalies induced by aerosol direct forcing: the role of the Tibetan Plateau, Clim. Dyn., 26, 855–864, doi:10.1007/s00382-006-0114-z, 2006.

Lawrence, M. G., and Lelieveld, J.: Atmospheric pollutant outflow from southern Asia: a review, Atmos. Chem. Phys., 10, 11017-11096, doi:10.5194/acp-10-11017-2010, 2010.

Lelieveld, J., Crutzen, P. J., Ramanathan, V., Andreae, M. O., Brenninkmeijer, C. A. M., Campos, T., Cass, G. R., Dickerson, R. R., Fischer, H., de Gouw, J. A., Hansel, A., Jefferson, A., Kley, D., de Laat, A. T. J., Lal, S., Lawrence, M. G., Lobert, J. M., Mayol-Bracero, O. L., Mitra, A. P., Novakov, T., Oltmans, S. J., Prather, K. A., Reiner, T., Rodhe, H., Scheeren, H. A., Sikka, D., and Williams, J.: The Indian Ocean Experiment: Widespread air pollution from South and Southeast Asia, Science, 291, 1031–1036, doi:10.1126/science.1057103, 2001.

Leon, J.-F., Chazette, P., Dulac, F., Pelon, J., Flamant, C., Bonazzola, M., Foret, G., Alfaro, S., Cachier, H., and Cautenet, S.: Large-scale advection of continental aerosols during INDOEX, J. Geophys. Res., 106, 28427–28428, 28439, 2001.

Li, Q., Jiang, J. H., Wu, D. L., Read, W. G., Livesey, N. J., Waters, J. W., Zhang, Y., Wang, B., Filipiak, M. J., and Davis, C. P.: Convective outflow of South Asian pollution: A global CTM simulation compared with EOS MLS observations, Geophys. Res. Lett., 32, L14826, doi:10.1029/2005GL022762, 2005.

Liao, H., Adams, P. J., Chung, S. H., Seinfeld, J. H., Mickley, L. J., and Jacob, D. J.: Interactions between tropospheric chemistry and aerosols in a unified general circulation model, J. Geophys. Res., 108, 4001, doi:10.1029/2001JD001260, 2003.

Liao, H., and Seinfeld, J. H.: Global impacts of gas-phase chemistry-aerosol

interactions on direct radiative forcing by anthropogenic aerosols and ozone, J. Geophys. Res., 110, D18208, doi:10.1029/2005JD005907, 2005.

Liao, H., Zhang, Y., Chen, W.-T., Raes, F., and Seinfeld, J. H.: Effect of chemistry-aerosol-climate coupling on predictions of future climate and future levels of tropospheric ozone and aerosols, J. Geophys. Res., 114, D10306, doi:10.1029/2008JD010984, 2009.

Liu, H., Jacob, D. J., Bey, I., and Yantosca, R. M.: Constraints from 210Pb and 7Be on wet deposition and transport in a global three-dimensional chemical tracer model driven by assimilated meteorological fields, J. Geophys. Res., 106, 12109–12128, 2001.

Liu, X., Penner, J. E., and Wang, M.: Influence of anthropogenic sulfate and black carbon on upper tropospheric clouds in the NCAR CAM3 model coupled to the IMPACT global aerosol model, J. Geophys. Res., 114, D03204, doi:10.1029/2008JD010492, 2009.

Livesey, N. J., Filipiak, M. J., Froidevaux, L., Read, W. G., Lambert, A., Santee, M. L., Jiang, J. H., Pumphrey, H. C., Waters, J. W., and Cofield, R. E.: Validation of Aura Microwave Limb Sounder O_3 and CO observations in the upper troposphere and lower stratosphere, J. Geophys. Res., 113, D15S02, doi:10.1029/2007JD008805, 2008.

Livesey, N. J., Read, W. G., Wagner, P. A., Froidevaux, L., Lambert, A., Manney, G. L., Pumphrey, H. C., Santee, M. L., Schwartz, M. J., Wang, S., Cofield, R. E., Cuddy, D. T., Fuller, R. A., Jarnot, R. F., Jiang, J. H., and Knosp, B. W.: Version 3.3 Level 2 data quality and description document, JPL D-33509, 2011.

Lodhi, A., Ghauri, B., Khan, M. R., Rahman, S., and Shafique, S.: Particulate matter ($PM_{2.5}$) concentration and source apportionment in Lahore, J. Brazil. Chem. Soc., 20, 1811–1820, 2009.

Lou, S., Liao, H., and Zhu, B.: Impacts of aerosols on surface-layer ozone concentrations in China through heterogeneous reactions and changes in photolysis rates, Atmos. Environ., 85, 123–138, 2014.

Ma, J., Tang, J., Li, S.-M., and Jacobson, M. Z.: Size distributions of ionic aerosols measured at Waliguan Observatory: Implication for nitrate gas-to-particle transfer processes in the free troposphere, J. Geophys. Res., 108, 4541, doi:10.1029/2002jd003356, 2003.

Martin, R. V., Jacob, D. J., Yantosca, R. M., Chin, M., and Ginoux, P.: Global and regional decreases in tropospheric oxidants from photochemical effects of aerosols, J. Geophys. Res., 108, 4097, doi:10.1029/2002JD002622, 2003.

McCormick, M. P.: SAGE II: an overview, Adv. Space Res., 7, 219-226, 1987.

McLinden, C., Olsen, S., Hannegan, B., Wild, O., Prather, M., and Sundet, J.: Stratospheric ozone in 3-D models: A simple chemistry and the cross-tropopause flux, J. Geophys. Res., 105, 14653–14665, doi:10.1029/2000JD900124, 2000.

Mickley, L. J., Murti, P., Jacob, D. J., Logan, J. A., Koch, D., and Rind, D.: Radiative forcing from tropospheric ozone calculated with a unified chemistry-climate model, J. Geophys. Res., 104, 30153-30172, 1999.

Ming, J., Zhang, D., Kang, S., and Tian, W.: Aerosol and fresh snow chemistry in the East Rongbuk Glacier on the northern slope of Mt. Qomolangma (Everest), J. Geophys. Res., 112, D15307, doi:10.1029/2007JD008618,

2007.

Momin, G. A., Rao, P. S. P., Safai, P. D., Ali, K., Naik, M. S., and Pillai, A. G.: Atmospheric aerosol characteristic studies at Pune and Thiruvananthapuram during INDOEX programme–1998, Curr. Sci., 76, 985-989, 1999.

Mu, Q., and Liao, H.: Simulation of the interannual variations of aerosols in China: role of variations in meteorological parameters, Atmos. Chem. Phys., 14, 9597–9612, 2014.

Murray, L. T., Jacob, D. J., Logan, J. A., Hudman, R. C., and Koshak, W. J.: Optimized regional and interannual variability of lightning in a global chemical transport model constrained by LIS/OTD satellite data, J. Geophys. Res., 117, D20307, doi:10.1029/2012JD017934, 2012.

Nair, P. R., George, S. K., Sunilkumar, S., Parameswaran, K., Jacob, S., and Abraham, A.: Chemical composition of aerosols over peninsular India during winter, Atmos. Environ., 40, 6477–6493, 2006.

Nair, V. S., Solmon, F., Giorgi, F., Mariotti, L., Babu, S. S., and Moorthy, K. K.: Simulation of South Asian aerosols for regional climate studies, J. Geophys. Res., 117, D04209, doi:10.1029/2011JD016711, 2012.

Nakamura, T., Matsumoto, K., and Uematsu, M.: Chemical characteristics of aerosols transported from Asia to the East China Sea: an evaluation of anthropogenic combined nitrogen deposition in autumn, Atmos. Environ., 39, 1749–1758, 2005.

Oberbeck, V. R., Livingston, J. M., Russell, P. B., Pueschel, R. F., Rosen, J. N., Osborn, M. T., Kritz, M. A., Snetsinger, K. G., and Ferry, G. V.: SAGE II aerosol validation: Selected altitude measurements, including particle micromeasurements, J. Geophys. Res., 94, 8367–8380, doi:10.1029/JD094iD06p08367, 1989.

Pant, P., Hegde, P., Dumka, U., Sagar, R., Satheesh, S., Moorthy, K. K., Saha, A., and Srivastava, M.: Aerosol characteristics at a high-altitude location in central Himalayas: Optical properties and radiative forcing, J. Geophys. Res., 111, D17206, doi:10.1029/2005JD006768, 2006.

Park, M., Randel, W. J., Kinnison, D. E., Garcia, R. R., and Choi, W.: Seasonal variation of methane, water vapor, and nitrogen oxides near the tropopause: Satellite observations and model simulations, J. Geophys. Res., 109, D03302, doi:10.1029/2003JD003706, 2004.

Park, M., Randel, W. J., Gettelman, A., Massie, S. T., and Jiang, J. H.: Transport above the Asian summer monsoon anticyclone inferred from Aura Microwave Limb Sounder tracers, J. Geophys. Res., 112, D16309, doi:10.1029/2006JD008294, 2007.

Park, M., Randel, W. J., Emmons, L. K., Bernath, P. F., Walker, K. A., and Boone, C. D.: Chemical isolation in the Asian monsoon anticyclone observed in Atmospheric Chemistry Experiment (ACE–FTS) data, Atmos. Chem. Phys., 8, 757–764, 2008.

Park, M., Randel, W. J., Emmons, L. K., and Livesey, N. J.: Transport pathways of carbon monoxide in the Asian summer monsoon diagnosed from Model of Ozone and Related Tracers (MOZART), J. Geophys. Res., 114, D08303, doi:10.1029/2008JD010621, 2009.

Park, R. J., Jacob, D. J., Chin, M., and Martin, R. V.: Sources of carbonaceous aerosols over the United States and implications for natural visibility, J. Geophys. Res., 108, 4355, doi:10.1029/2002JD003190, 2003.

Park, R. J., Jacob, D. J., Field, B. D., Yantosca, R. M., and Chin, M.: Natural and transboundary pollution influences on sulfate–nitrate–ammonium aerosols in the United States: Implications for policy, J. Geophys. Res., 109, D15204, doi:10.1029/2003JD004473, 2004.

Pitari, G., Aquila, V., Kravitz, B., Robock, A., Watanabe, S., Cionni, I., Luca, N. D., Genova, G. D., Mancini, E., and Tilmes, S.: Stratospheric ozone response to sulfate geoengineering: Results from the Geoengineering Model Intercomparison Project (GeoMIP), J. Geophys. Res., 119, 2629–2653, doi: 10.1002/2013JD020566, 2014.

Popp, P., Marcy, T., Jensen, E., Kärcher, B., Fahey, D., Gao, R., Thompson, T., Rosenlof, K., Richard, E., and Herman, R.: The observation of nitric acid-containing particles in the tropical lower stratosphere, Atmos. Chem. Phys., 6, 601-611, 2006.

Pye, H., Liao, H., Wu, S., Mickley, L. J., Jacob, D. J., Henze, D. K., and Seinfeld, J.: Effect of changes in climate and emissions on future sulfate–nitrate–ammonium aerosol levels in the United States, J. Geophys. Res., 114, D01205, doi:10.1029/2008JD010701, 2009.

Qie, X., Wu, X., Yuan, T., Bian, J., and Lü, D.: Comprehensive Pattern of Deep Convective Systems over the Tibetan Plateau–South Asian Monsoon Region Based on TRMM Data, J. Clim., 27, 6612–6626, 2014.

Ram, K., Sarin, M., and Hegde, P.: Atmospheric abundances of primary and secondary carbonaceous species at two high-altitude sites in India: Sources and temporal variability, Atmos. Environ., 42, 6785-6796, 2008.

Ramanathan, V., Li, F., Ramana, M., Praveen, P., Kim, D., Corrigan, C., Nguyen, H., Stone, E. A., Schauer, J. J., and Carmichael, G.: Atmospheric brown clouds: Hemispherical and regional variations in long-range transport, absorption, and radiative forcing, J. Geophys. Res., 112, D22S21, doi:10.1029/2006JD008124, 2007.

Randel, W. J., and Park, M.: Deep convective influence on the Asian summer monsoon anticyclone and associated tracer variability observed with Atmospheric Infrared Sounder (AIRS), J. Geophys. Res., 111, D12314, doi:10.1029/2005JD006490, 2006.

Randel, W. J., Park, M., Emmons, L., Kinnison, D., Bernath, P., Walker, K. A., Boone, C., and Pumphrey, H.: Asian monsoon transport of pollution to the stratosphere, Science, 328, 611–613, 2010.

Rasch, P. J., Tilmes, S., Turco, R. P., Robock, A., Oman, L., Chen, C. C., Stenchikov, G. L., and Garcia, R. R.: An overview of geoengineering of climate using stratospheric sulphate aerosols, Philos. Trans. R. Soc. A-Math. Phys. Eng. Sci., 366, 4007-4037, doi:10.1098/rsta.2008.0131, 2008.

Rastogi, N., and Sarin, M.: Long-term characterization of ionic species in aerosols from urban and high-altitude sites in western India: Role of mineral dust and anthropogenic sources, Atmos. Environ., 39, 5541–5554, 2005.

Rastogi, N., and Sarin, M.: Quantitative chemical composition and characteristics of aerosols over western India: one-year record of temporal variability, Atmos. Environ., 43, 3481–3488, 2009.

Rengarajan, R., Sarin, M., and Sudheer, A.: Carbonaceous and inorganic species in atmospheric aerosols during wintertime over urban and high-altitude sites in North India, J. Geophys. Res., 112, D21307,

doi:10.1029/2006JD008150, 2007.

Russell, P. B., and Mccormick, M. P.: SAGE II aerosol data validation and initial data use: An introduction and overview, J. Geophys. Res., 94, 8335–8338, 1989.

Safai, P., Kewat, S., Praveen, P., Rao, P., Momin, G., Ali, K., and Devara, P.: Seasonal variation of black carbon aerosols over a tropical urban city of Pune, India, Atmos. Environ., 41, 2699–2709, 2007.

Salam, A., Bauer, H., Kassin, K., Mohammad Ullah, S., and Puxbaum, H.: Aerosol chemical characteristics of a mega-city in Southeast Asia (Dhaka–Bangladesh), Atmos. Environ., 37, 2517–2528, 2003.

Santee, M., Lambert, A., Read, W., Livesey, N., Cofield, R., Cuddy, D., Daffer, W., Drouin, B., Froidevaux, L., and Fuller, R.: Validation of the Aura Microwave Limb Sounder HNO_3 measurements, J. Geophys. Res., 112, D24S40, doi:10.1029/2007JD008721, 2007.

Sauvage, B., Martin, R., Donkelaar, A. v., Liu, X., Chance, K., Jaeglé, L., Palmer, P., Wu, S., and Fu, T.-M.: Remote sensed and in situ constraints on processes affecting tropical tropospheric ozone, Atmos. Chem. Phys., 7, 815–838, 2007.

Seinfeld, J. H., and Pandis, S. N.: Atmospheric chemistry and physics: from air pollution to climate change, Environment Science & Policy for Sustainable Development, 51, 212–214(213), 2006.

Sharma, R. K., Bhattarai, B., Sapkota, B., Gewali, M., and Kjeldstad, B.: Black carbon aerosols variation in Kathmandu valley, Nepal, Atmos. Environ., 63, 282–288, doi:10.1016/j.atmosenv.2012.09.023, 2012.

Shrestha, A. B., Wake, C. P., Dibb, J. E., Mayewski, P. A., Whitlow, S. I., Carmichael, G. R., and Ferm, M.: Seasonal variations in aerosol concentrations and compositions in the Nepal Himalaya, Atmos. Environ., 34, 3349–3363, 10.1016/s1352-2310(99)00366-0, 2000.

Š kerlak, B., Sprenger, M., and Wernli, H.: A global climatology of stratosphere-troposphere exchange using the ERA-Interim data set from 1979 to 2011, Atmos. Chem. Phys, 14, 913–937, 2014.

Stevenson, D. S., Dentener, F. J., Schultz, M. G., Ellingsen, K., Van Noije, T. P. C., Wild, O., Zeng, G., Amann, M., Atherton, C. S., and Bell, N.: Multimodel ensemble simulations of present-day and near-future tropospheric ozone, J. Geophys. Res., 111, D08301, doi:10.1029/2005JD006338, 2006.

Streets, D. G., Bond, T. C., Carmichael, G. R., Fernandes, S. D., Fu, Q., He, D., Klimont, Z., Nelson, S. M., Tsai, N. Y., and Wang, M. Q.: An inventory of gaseous and primary aerosol emissions in Asia in the year 2000, J. Geophys. Res., 108, GTE 30–31, 2003.

Su, H., Jiang, J. H., Lu, X. H., Penner, J. E., Read, W. G., Massie, S., Schoeberl, M. R., Colarco, P., Livesey, N. J., and Santee, M. L.: Observed Increase of TTL Temperature and Water Vapor in Polluted Clouds over Asia, J. Clim., 24, 2728–2736, 10.1175/2010jcli3749.1, 2011.

Sudheer, A., and Sarin, M.: Carbonaceous aerosols in MABL of Bay of Bengal: Influence of continental outflow, Atmos. Environ., 42, 4089-4100, 2008.

Talukdar, R. K., Burkholder, J. B., Roberts, J. M., Portmann, R. W., and Ravishankara, A.: Heterogeneous Interaction of N_2O_5 with HCl Doped H_2SO_4 under Stratospheric Conditions: $ClNO_2$ and Cl_2 Yields, J. Phys. Chem. A., 116, 6003–6014, 2012.

Tang, M., Telford, P., Pope, F., Rkiouak, L., Abraham, N., Archibald, A., Braesicke, P., Pyle, J., McGregor, J., and Watson, I.: Heterogeneous reaction of N_2O_5 with airborne TiO_2 particles and its implication for stratospheric particle injection, Atmos. Chem. Phys., 14, 6035–6048, 2014.

Tare, V., Tripathi, S., Chinnam, N., Srivastava, A., Dey, S., Manar, M., Kanawade, V. P., Agarwal, A., Kishore, S., and Lal, R.: Measurements of atmospheric parameters during Indian Space Research Organization Geosphere Biosphere Program Land Campaign II at a typical location in the Ganga Basin: 2. chemical properties, J. Geophys. Res., 111, D23210, doi:10.1029/2006JD007279, 2006.

Thornton, J. A., Jaeglé, L., and McNeill, V. F.: Assessing known pathways for HO_2 loss in aqueous atmospheric aerosols: Regional and global impacts on tropospheric oxidants, J. Geophys. Res., 113, D05303, doi:10.1029/2007JD009236, 2008.

Tobo, Y., Zhang, D., Iwasaka, Y., and Shi, G.: On the mixture of aerosols and ice clouds over the Tibetan Plateau: Results of a balloon flight in the summer of 1999, Geophys. Res. Lett., 34, L23801, doi:10.1029/2007GL031132, 2007.

Tripathi, S., Dey, S., Tare, V., and Satheesh, S.: Aerosol black carbon radiative forcing at an industrial city in northern India, Geophys. Res. Lett., 32, L08802, doi:10.1029/2005GL022515, 2005.

van der Werf, G. R., Randerson, J. T., Giglio, L., Collatz, G. J., Mu, M., Kasibhatla, P. S., Morton, D. C., DeFries, R. S., Jin, Y., and van Leeuwen, T. T.: Global fire emissions and the contribution of deforestation, savanna, forest, agricultural, and peat fires (1997–2009), Atmos. Chem. Phys., 10, 11707–11735, 2010.

Vanhellemont, F., Tetard, C., Bourassa, A., Fromm, M., Dodion, J., Fussen, D., Brogniez, C., Degenstein, D., Gilbert, K., and Turnbull, D.: Aerosol extinction profiles at 525 nm and 1020 nm derived from ACE imager data: comparisons with GOMOS, SAGE II, SAGE III, POAM III, and OSIRIS, Atmos. Chem. Phys., 8, 2027-2037, 2008.

Venkataraman, C., Reddy, C. K., Josson, S., and Reddy, M. S.: Aerosol size and chemical characteristics at Mumbai, India, during the INDOEX-IFP (1999), Atmos. Environ., 36, 1979–1991, 2002.

Verma, S., Boucher, O., Reddy, M., Upadhyaya, H., Van, P., Binkowski, F., and Sharma, O.: Tropospheric distribution of sulphate aerosols mass and number concentration during INDOEX-IFP and its transport over the Indian Ocean: a GCM study, Atmos. Chem. Phys., 12, 6185–6196, 2012.

Vernier, J.-P., Pommereau, J.-P., Garnier, A., Pelon, J., Larsen, N., Nielsen, J., Christensen, T., Cairo, F., Thomason, L., and Leblanc, T.: Tropical stratospheric aerosol layer from CALIPSO lidar observations, J. Geophys. Res., 114, D00H10, doi:10.1029/2009JD011946, 2009.

Vernier, J. P., Thomason, L., and Kar, J.: CALIPSO detection of an Asian tropopause aerosol layer, Geophys. Res. Lett., 38, L07804, doi:10.1029/2010GL046614, 2011.

Voigt, C., Schreiner, J., Kohlmann, A., Zink, P., Mauersberger, K., Larsen, N., Deshler, T., Kröger, C., Rosen, J., and Adriani, A.: Nitric acid trihydrate (NAT) in polar stratospheric clouds, Science, 290, 1756-1758, 2000.

Wang, P., McCormick, M., McMaster, L., Chu, W., Swissler, T., Osborn, M.,

Russell, P., Oberbeck, V., Livingston, J., and Rosen, J.: SAGE II aerosol data validation based on retrieved aerosol model size distribution from SAGE II aerosol measurements, J. Geophys. Res., 94, 8381–8393, doi:10.1029/JD094iD06p08381, 1989.

Wang, Y., Logan, J. A., and Jacob, D. J.: Global simulation of tropospheric O_3–NO_x–hydrocarbon chemistry: 2. Model evaluation and global ozone budget, J. Geophys. Res., 103, 10727–10755, 1998.

Wang, Y., Zhang, Q., He, K., Zhang, Q., and Chai, L.: Sulfate-nitrate-ammonium aerosols over China: response to 2000–2015 emission changes of sulfur dioxide, nitrogen oxides, and ammonia, Atmos. Chem. Phys., 13, 2635–2652, 2013.

Waters, J. W., Froidevaux, L., Harwood, R. S., Jarnot, R. F., Pickett, H. M., Read, W. G., Siegel, P. H., Cofield, R. E., Filipiak, M. J., and Flower, D.: The earth observing system microwave limb sounder (EOS MLS) on the Aura satellite, IEEE T. Geosci. Remote., 44, 1075-1092, 2006.

Weigel, R., Borrmann, S., Kazil, J., Minikin, A., Stohl, A., Wilson, J., Reeves, J., Kunkel, D., De Reus, M., and Frey, W.: In situ observations of new particle formation in the tropical upper troposphere: the role of clouds and the nucleation mechanism, Atmos. Chem. Phys. Discuss., 11, 2011.

Wesely, M.: Parameterization of surface resistances to gaseous dry deposition in regional-scale numerical models, Atmos. Environ., 23, 1293-1304, 1989.

Wu, L. T., Su, H., and Jiang, J. H.: Regional simulations of deep convection and biomass burning over South America: 2. Biomass burning aerosol effects on clouds and precipitation, J. Geophys. Res., 116, doi:10.1029/2011jd01 6106, 2011.

Wu, S., Mickley, L. J., Jacob, D. J., Logan, J. A., Yantosca, R. M., and Rind, D.: Why are there large differences between models in global budgets of tropospheric ozone? J. Geophys. Res., 112, D05302, doi:10.1029/2006JD007801, 2007.

Wu, S., Mickley, L. J., Jacob, D. J., Rind, D., and Streets, D. G.: Effects of 2000–2050 changes in climate and emissions on global tropospheric ozone and the policy–relevant background surface ozone in the United States, J. Geophys. Res., 113, D18312, doi:10.1029/2007JD009639, 2008.

Xia, X., Zong, X., Cong, Z., Chen, H., Kang, S., and Wang, P.: Baseline continental aerosol over the central Tibetan plateau and a case study of aerosol transport from South Asia, Atmos. Environ., 45, 7370-7378, 2011.

Xiong, X., Houweling, S., Wei, J., Maddy, E., Sun, F., and Barnet, C.: Methane plume over south Asia during the monsoon season: satellite observation and model simulation, Atmos. Chem. Phys., 9, 783-794, 2009.

Yanai, M., Li, C., and Song, Z.: Seasonal heating of the Tibetan Plateau and its effects on the evolution of the Asian summer monsoon, J. Meteorol. Soc. Jan., 70, 319–351, 1992.

Yao, X., Chan, C. K., Fang, M., Cadle, S., Chan, T., Mulawa, P., He, K., and Ye, B.: The water-soluble ionic composition of $PM_{2.5}$ in Shanghai and Beijing, China, Atmos. Environ., 36, 4223–4234, 2002.

Yin, Y., Chen, Q., Jin, L., Chen, B., Zhu, S., and Zhang, X.: The effects of deep convection on the concentration and size distribution of aerosol particles within the upper troposphere: A case study, J. Geophys. Res., 117,

D22202, doi:10.1029/2012JD017827, 2012.

Zeng, G., Pyle, J., and Young, P.: Impact of climate change on tropospheric ozone and its global budgets, Atmos. Chem. Phys., 8, 369-387, 2008.

Zhang, G. J., and McFarlane, N. A.: Sensitivity of climate simulations to the parameterization of cumulus convection in the Canadian Climate Centre general circulation model, Atmos.-Ocean, 33, 407–446, 1995.

Zhang, L., Liao, H., and Li, J.: Impacts of Asian summer monsoon on seasonal and interannual variations of aerosols over eastern China, J. Geophys. Res., 115, D00K05, doi:10.1029/2009JD012299, 2010.

Zhang, N., Cao, J., Ho, K., and He, Y.: Chemical characterization of aerosol collected at Mt. Yulong in wintertime on the southeastern Tibetan Plateau, Atmos. Res., 107, 76, 2012.

Zhang, Q., Streets, D. G., Carmichael, G. R., He, K., Huo, H., Kannari, A., Klimont, Z., Park, I., Reddy, S., and Fu, J.: Asian emissions in 2006 for the NASA INTEX-B mission, Atmos. Chem. Phys., 9, 5131–5153, 2009.

Zhang, X., Cao, J., Li, L., Arimoto, R., Cheng, Y., Huebert, B., and Wang, D.: Characterization of atmospheric aerosol over Xian in the south margin of the Loess Plateau, China, Atmos. Environ., 36, 4189–4199, 2002.

Zhang, X. Y., Wang, Y. Q., Niu, T., Zhang, X. C., Gong, S. L., Zhang, Y. M., and Sun, J. Y.: Atmospheric aerosol compositions in China: spatial/temporal variability, chemical signature, regional haze distribution and comparisons with global aerosols, Atmos. Chem. Phys., 12, 779–799, doi:10.5194/acp-12-779-2012, 2012.

Zhang, Y., Dore, A., Ma, L., Liu, X., Ma, W., Cape, J., and Zhang, F.: Agricultural ammonia emissions inventory and spatial distribution in the North China Plain, Environ. Pollut., 158, 490–501, 2010.

Zhao, X., Turco, R. P., Kao, C. Y. J., and Elliott, S.: Aerosol-induced chemical perturbations of stratospheric ozone: Three-dimensional simulations and analysis of mechanisms, J. Geophys. Res., 102, 3617–3637, doi:10.1029/96jd03406, 1997.

Zhu, J., Liao, H., and Li, J.: Increases in aerosol concentrations over eastern China due to the decadal-scale weakening of the East Asian summer monsoon, Geophys. Res. Lett., 39, L09809, doi:10.1029/2012GL051428, 2012.

1308 Table 1. Summary of Annual Emissions of Aerosols and Aerosol
1309 Precursors in Asia (60°E-155°E, 10°N-55°N)

Species	Global	Asia
NO_x (Tg N yr^{-1})		
Aircraft	0.5	0.08
Anthropogenic	28.6	9.96
Biomass burning	4.7	0.27
Fertilizer	0.7	0.31
Lightning	5.9	0.87
Soil	5.9	0.96
Total	46.3	12.45
SO_2 (Tg S yr^{-1})		
Aircraft	0.1	0.01
Anthropogenic	52.6	23.46
Biomass burning	1.2	0.07
Volcanoes	4.4	1.04
No_eruption	8.9	1.78
Ship	7.4	0.94
Total	74.6	27.30
NH_3 (Tg N yr^{-1})		
Anthropogenic	34.9	17.83
Natural	14.2	2.01
Biomass burning	3.5	0.21
Biofuel	1.6	0.71
Total	54.2	20.76
OC (Tg C yr^{-1})		
Anthropogenic	3.1	1.42
Biomass burning	18.7	1.10
Biofuel	6.3	3.28
Biogenic	9.7	1.22
Total	37.8	7.02
BC (Tg C yr^{-1})		
Anthropogenic	3.0	1.43
Biomass burning	2.2	0.12
Biofuel	1.6	0.86
Total	6.8	2.41

Table 2. Simulated seasonal mean concentrations of aerosols and their contributions to $PM_{2.5}$ (in percentages in parentheses) during summertime (June-August) of 2005 for the TP/SASM, TP, and SASM regions. The unit is $\mu g\ m^{-3}$ for concentrations at the surface, and $10^{-2}\ \mu g\ m^{-3}$ for concentrations at 200 hPa and 100 hPa.

	$PM_{2.5}$	SO_4^{2-}	NO_3^-	NH_4^+	OC	BC
			TP/SASM			
Surface	4.73	1.70(35.9%)	0.94(19.8%)	0.85(18.1%)	0.94(19.8%)	0.30(6.4%)
200 hPa	16.19	3.27(20.2%)	7.57(46.8%)	2.67(16.5%)	2.22(13.7%)	0.44(2.7%)
100 hPa	12.14	2.60(21.4%)	6.90(56.8%)	1.43(11.8%)	1.05(8.6%)	0.16(1.3%)
			TP			
Surface	5.44	2.12(39.0%)	1.05(19.3%)	1.08(19.9%)	0.88(16.1%)	0.31(5.7%)
200 hPa	19.80	4.16(21.0%)	9.43(47.6%)	3.25(16.4%)	2.49(12.6%)	0.47(2.4%)
100 hPa	10.58	2.60(24.6%)	5.51(52.0%)	1.35(12.7%)	0.99(9.4%)	0.14(1.3%)
			SASM			
Surface	4.02	1.28(31.8%)	0.83(20.5%)	0.63(15.6%)	1.00(24.8%)	0.29(7.2%)
200 hPa	12.57	2.38(18.9%)	5.72(45.5%)	2.10(16.7%)	1.95(15.5%)	0.41(3.3%)
100 hPa	13.71	2.60(19.0%)	8.30(60.5%)	1.52(11.1%)	1.11(8.1%)	0.18(1.3%)

Table 3. Sensitivity simulations to examine the impacts of uncertainties in surface-layer aerosol concentrations on simulated NO_3^- in the UTLS. "Conc" and "Ctri" denote, respectively, simulated seasonal mean concentrations of SO_4^{2-}, NO_3^-, NH_4^+, OC, BC and their contributions to $PM_{2.5}$ (in percentages) during summertime (June-August) of 2005. The mass concentrations are averaged over the TP/SASM region, with unit of $\mu g\ m^{-3}$ at the surface layer and of $10^{-2}\ \mu g\ m^{-3}$ at 200 hPa and 100 hPa. Also shown are the NMBs, as the simulated surface-layer concentrations are compared with measurements described in Section 4.2.

Species	Baseline Case			SO$_2$ (+20%)			NO$_x$ (-50%)			NH$_3$ (-50%)			All Change		
	Conc.	Ctri.	NMB	Conc.	Ctri.	NMB	Conc.	Ctri.	NMB	Conc.	Ctri.	NMB	Conc.	Ctri.	NMB
Surface															
SO_4^{2-}	1.70	35.9%	−14.7%	1.92	38.1%	−4.4%	1.58	39.5%	−18.1%	1.70	38.1%	−14.7%	1.78	43.2%	−8.3%
NO_3^-	0.94	19.8%	+51.5%	0.94	18.7%	+53.5%	0.50	12.5%	−11.7%	0.73	16.4%	+24.1%	0.39	9.5%	−27.0%
NH_4^+	0.85	18.1%	+74.9%	0.94	18.6%	+93.8%	0.68	17.1%	+44.1%	0.78	17.6%	+64.6%	0.71	17.3%	+55.4%
OC	0.94	19.8%	−57.2%	0.94	18.6%	−57.2%	0.94	23.4%	−57.2%	0.94	21.0%	−57.2%	0.94	22.7%	−57.2%
BC	0.30	6.4%	−32.2%	0.30	6.0%	−32.2%	0.30	7.5%	−32.2%	0.30	6.8%	−32.2%	0.30	7.3%	−32.2%
200 hPa															
SO_4^{2-}	3.27	20.2%		3.67	22.9%		3.31	20.6%		3.29	29.1%		3.74	33.7%	
NO_3^-	7.57	46.8%		7.05	43.9%		7.41	46.0%		3.86	34.2%		3.19	28.7%	
NH_4^+	2.67	16.5%		2.67	16.6%		2.71	16.8%		1.49	13.2%		1.50	13.5%	
OC	2.22	13.7%		2.22	13.8%		2.22	13.8%		2.22	19.7%		2.22	20.0%	
BC	0.44	2.7%		0.44	2.7%		0.44	2.7%		0.44	3.9%		0.44	4.0%	
100 hPa															
SO_4^{2-}	2.60	21.4%		2.80	23.0%		2.66	21.9%		2.60	25.2%		2.87	27.2%	
NO_3^-	6.90	56.8%		6.72	55.3%		6.81	56.1%		5.68	55.0%		5.62	53.3%	
NH_4^+	1.43	11.8%		1.43	11.7%		1.45	12.0%		0.84	8.1%		0.84	8.0%	
OC	1.05	8.6%		1.05	8.6%		1.05	8.7%		1.05	10.2%		1.05	10.0%	
BC	0.16	1.3%		0.16	1.3%		0.16	1.3%		0.16	1.6%		0.16	1.5%	

Figure Captions

Figure. 1. Regions examined in this study: the Tibetan Plateau region (TP, 70–105°E, 25–40°N), the SASM region (SASM, 70–105°E, 10–25°N), and the anticyclone region of (20–120°E, 10–40°N).

Figure. 2. Monthly variations in emissions of NO_x (Tg N month^{-1}), SO_2 (Tg S month^{-1}), NH_3 (Tg N month^{-1}), OC (Tg C month^{-1}), and BC (Tg C month^{-1}) over Asia. Values shown are the total emissions (anthropogenic plus natural emissions listed in Table 1).

Figure. 3. Simulated global distributions of surface-layer HNO_3 (pptv) and O_3 (ppbv) averaged over June-August, 2005.

Figure. 4. Comparisons of simulated HNO_3 concentrations (pptv) with observations (pptv) from MLS. (a) and (b) are simulated concentrations at 200 hPa and 100 hPa, respectively. (c) is the latitude-altitude cross section of simulated HNO_3 concentrations averaged over 70–105°E. (d)-(f) are the same as (a)-(c), except that (d)-(f) are observations from MLS. The white areas in (d) and (f) have no datasets available from MLS. All the datasets are averaged over June-August of 2005.

Figure. 5. Comparisons of simulated O_3 concentrations (ppbv) with observations (ppbv) from MLS. (a) and (b) are simulated concentrations at 200 hPa and 100 hPa, respectively. (c) is the latitude-altitude cross section of simulated O_3 concentrations averaged over 70–105°E. (d)-(f) are the same as (a)-(c), except that (d)-(f) are observations from MLS. All the datasets are averaged over June-August of 2005.

Figure. 6. The simulated and observed vertical profiles of monthly mean O_3 mixing ratios at (a) Kunming and (b) Lhasa in August. The model results are from the simulation of year 2005. The observations in Kunming were conducted during August 7–13 (11 profiles of O_3 collected) in 2009 and during August 12–31 in 2012 (daily observations). The observations in Lhasa were conducted during August 22–28 in 2010 (12 profiles of O_3 collected) and during August 4–26 in 2013 (daily observations).

Figure. 7. Simulated seasonal mean concentrations (µg m^{-3}) of sulfate, nitrate, ammonium, organic carbon, black carbon, and $PM_{2.5}$ at (a) the surface layer, (b) 200 hPa, and (c) 100 hPa, during summer (June-August) of year 2005. Note that color bars are different for concentrations at the surface, 200 hPa, and 100 hPa.

Figure. 8. (a) Locations with measured aerosol concentrations from previous studies. Also shown are surface winds during summertime. (b)–(f) show the comparisons of simulated seasonal mean concentrations of sulfate, nitrate, ammonium, OC, and BC with measured values, respectively. Also shown in (b)–(f) are the 1:1 line (dashed), linear fit (solid line and equation), correlation coefficient between simulated and measured concentrations (R), and

1368 normalized mean bias (NMB) (defined as NMB=$\frac{\sum_{i=1}^{n}(P_i - O_i)}{\sum_{i=1}^{n} O_i}$ ×100%, where P_i

1369 and O_i are predicted and observed concentrations at station i for each aerosol

1370 species).

1371

1372 **Figure. 9.** (a) Monthly mean distribution of aerosol extinction coefficients (km^{-1})

1373 at 100 hPa for July of 2005. (b) Monthly mean vertical distributions of aerosol

1374 extinction coefficients (at 525 nm for SAGE II and 550 nm for GEOS-Chem)

1375 (km^{-1}) averaged over the Asian monsoon anticyclone region (20–120°E,

1376 10–40°N) for July of 2005. The horizontal dashed line represents the

1377 tropopause averaged over the Asian monsoon anticyclone region simulated by

1378 the GEOS-Chem model.

1379

1380 **Figure. 10.** Simulated contributions of nitrate to PM$_{2.5}$ (C$_{NIT}$= [NIT]/ [PM$_{2.5}$]

1381 ×100%) averaged over summer (June-August) of year 2005 at (a)

1382 surface-layer, (b) 200 hPa, and (c) 100 hPa. (d) The latitude-altitude cross

1383 section of simulated C$_{NIT}$ (%) averaged over 70–105°E.

1384

1385 **Figure. 11.** Latitude-altitude cross sections of simulated concentrations (color

1386 shades, μg m^{-3}) of SO_4^{2-} and NO_3^- averaged over 70–105°E in June-August

1387 of 2005, together with the wind vectors obtained from the European Centre for

1388 Medium-Range Weather Forecasts (ECMWF) ERA-Interim Reanalysis data.

1389 The black line is the tropopause simulated by the GEOS-Chem model.

1390

1391 **Figure. 12.** (a)-(b) Distributions of RH (%) and temperature (K) at 100 hPa.

1392 (c)-(d) The latitude-altitude cross sections of RH (%) and temperature (K)

1393 averaged over 70–105°E. RH and temperature are from the GEOS5

1394 assimilated meteorological fields, and all the values are the averages over

1395 June-August of year 2005.

1396

1397 **Figure. 13.** Mass budget for nitrate aerosol within the selected box of

1398 (70–105°E, 10–40°N, 8–16 km). E/W transport indicates net mass flux through

1399 the east and west lateral boundaries, N/S transport indicates net mass flux

1400 through the north and south lateral boundaries, and upward transport is the net

1401 mass flux through the top and bottom sides of the box. The mass flux is

1402 positive if it increases nitrate mass within the box. Unit of fluxes is Tg season^{-1}.

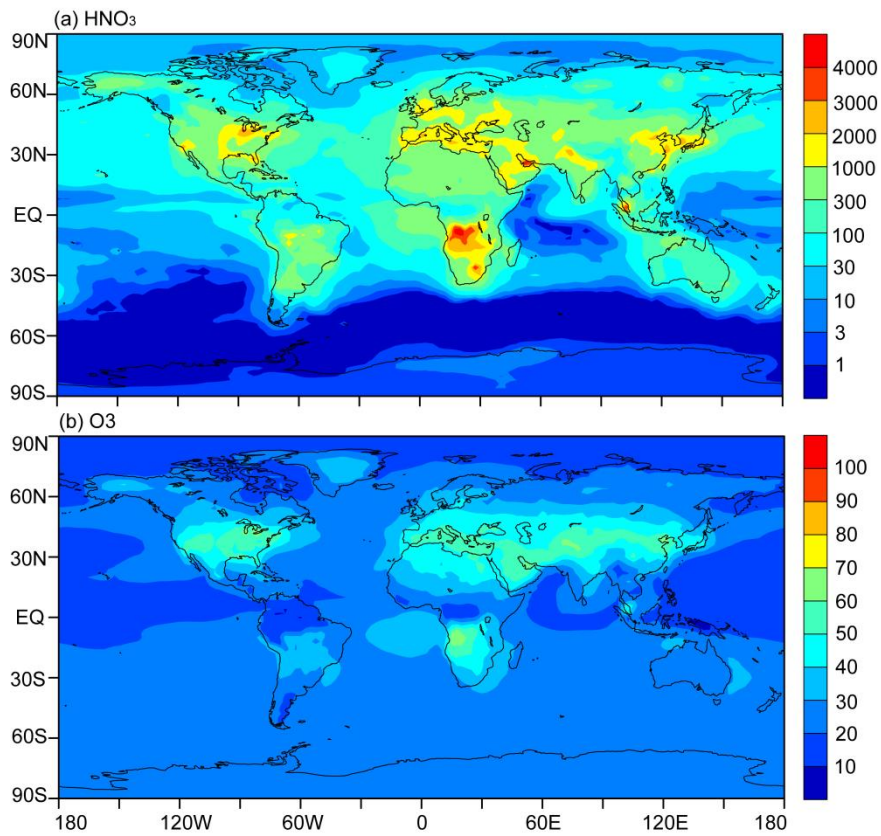1403 All the values are the averages over June-August of 2005.

Figure. 1. Regions examined in this study: the Tibetan Plateau region (TP, 70–105°E, 25–40°N), the SASM region (SASM, 70–105°E, 10–25°N), and the anticyclone region of (20–120°E, 10–40°N).
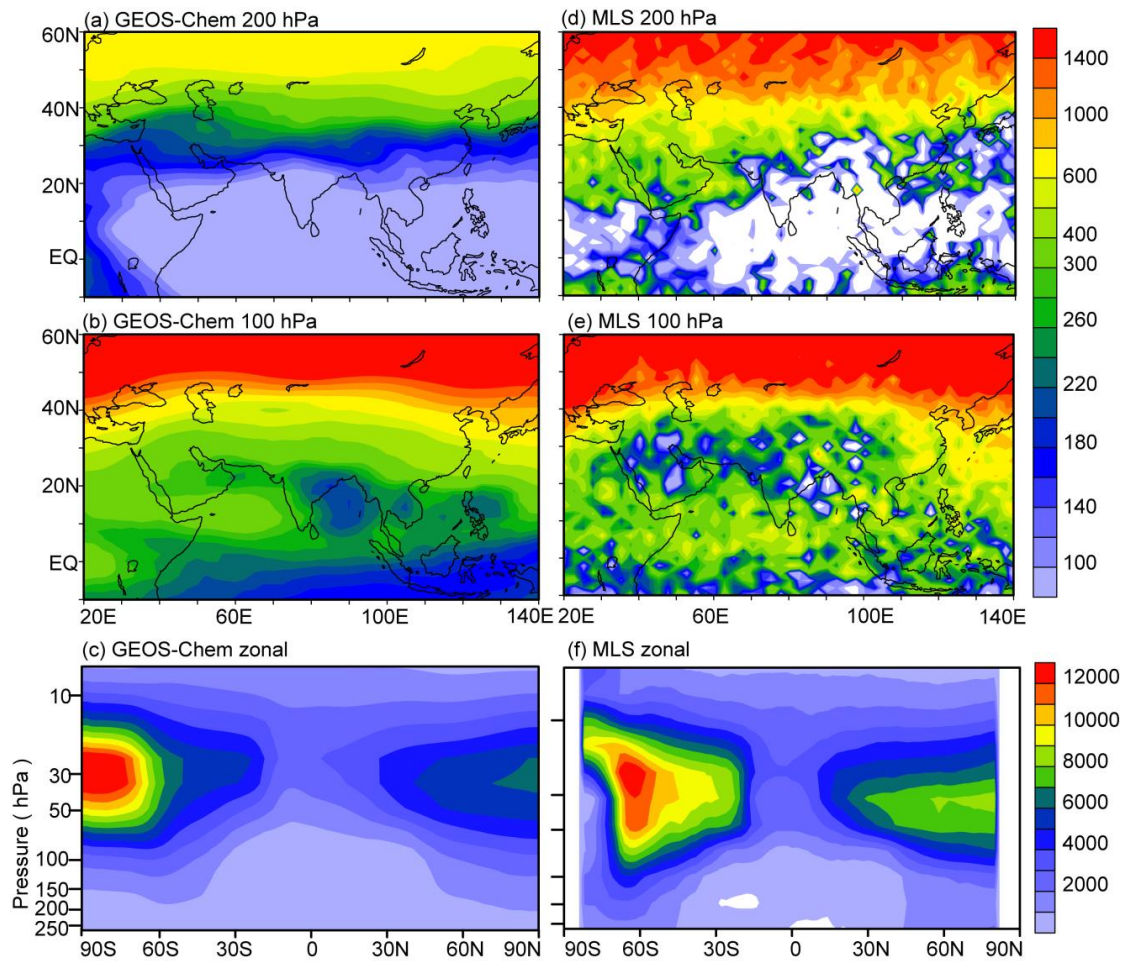
1409
1410
1411 **Figure. 2.** Monthly variations in emissions of NO_x (Tg N month^{-1}), SO_2 (Tg S
1412 month^{-1}), NH_3 (Tg N month^{-1}), OC (Tg C month^{-1}), and BC (Tg C month^{-1})
1413 over Asia. Values shown are the total emissions (anthropogenic plus natural
1414 emissions listed in Table 1).

1415
1416
Figure. 3. Simulated global distributions of surface-layer HNO_3 (pptv) and O_3
(ppbv) averaged over June-August, 2005.

Figure. 4. Comparisons of simulated HNO$_3$ concentrations (pptv) with observations (pptv) from MLS. (a) and (b) are simulated concentrations at 200 hPa and 100 hPa, respectively. (c) is the latitude-altitude cross section of simulated HNO$_3$ concentrations averaged over 70−105°E. (d)-(f) are the same as (a)-(c), except that (d)-(f) are observations from MLS. The white areas in (d) and (f) have no datasets available from MLS. All the datasets are averaged over June-August of 2005.

Figure. 5. Comparisons of simulated O_3 concentrations (ppbv) with observations (ppbv) from MLS. (a) and (b) are simulated concentrations at 200 hPa and 100 hPa, respectively. (c) is the latitude-altitude cross section of simulated O_3 concentrations averaged over 70−105°E. (d)-(f) are the same as (a)-(c), except that (d)-(f) are observations from MLS. All the datasets are averaged over June-August of 2005.

Figure 6. The simulated and observed vertical profiles of monthly mean O_3 mixing ratios at (a) Kunming and (b) Lhasa in August. The model results are from the simulation of year 2005. The observations in Kunming were conducted during August 7–13 (11 profiles of O_3 collected) in 2009 and during August 12–31 in 2012 (daily observations). The observations in Lhasa were conducted during August 22–28 in 2010 (12 profiles of O_3 collected) and during August 4–26 in 2013 (daily observations).

1445
1446

Figure. 7. Simulated seasonal mean concentrations (μg m^{-3}) of sulfate, nitrate,
ammonium, organic carbon, black carbon, and PM$_{2.5}$ at (a) the surface layer, (b)
200 hPa, and (c) 100 hPa, during summer (June-August) of year 2005. Note
that color bars are different for concentrations at the surface, 200 hPa, and 100
hPa.

Figure. 8. (a) Locations with measured aerosol concentrations from previous studies. Also shown are surface winds during summertime. (b)−(f) show the comparisons of simulated seasonal mean concentrations of sulfate, nitrate, ammonium, OC, and BC with measured values, respectively. Also shown in (b)−(f) are the 1:1 line (dashed), linear fit (solid line and equation), correlation coefficient between simulated and measured concentrations (R), and normalized mean bias (NMB) (defined as NMB=$\frac{\sum_{i=1}^{n}(P_i-O_i)}{\sum_{i=1}^{n}O_i}$ ×100%, where P_i and O_i are predicted and observed concentrations at station i for each aerosol species).

Figure. 9. (a) Monthly mean distribution of aerosol extinction coefficients (km^{-1}) at 100 hPa for July of 2005. (b) Monthly mean vertical distributions of aerosol extinction coefficients (at 525 nm for SAGE II and 550 nm for GEOS-Chem) (km^{-1}) averaged over the Asian monsoon anticyclone region (20$-$120°E, 10$-$40°N) for July of 2005. The horizontal dashed line represents the tropopause averaged over the Asian monsoon anticyclone region simulated by the GEOS-Chem model.

Figure. 10. Simulated contributions of nitrate to PM$_{2.5}$ (C$_{NIT}$= [NIT]/ [PM$_{2.5}$] ×100%) averaged over summer (June-August) of year 2005 at (a) surface-layer, (b) 200 hPa, and (c) 100 hPa. (d) The latitude-altitude cross section of simulated C$_{NIT}$ (%) averaged over 70−105°E.
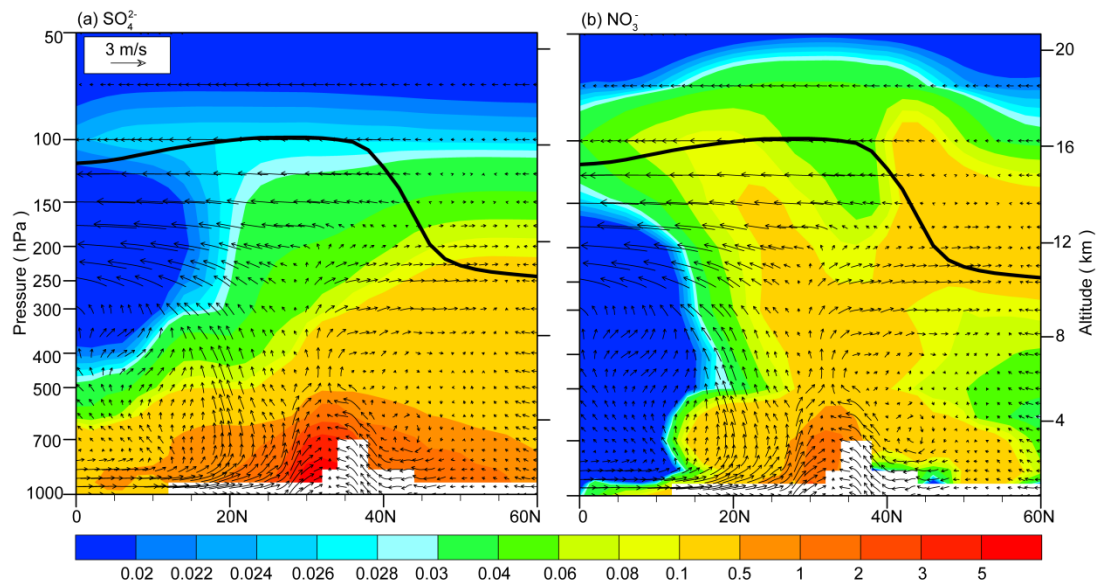
Figure. 11. Latitude-altitude cross sections of simulated concentrations (color shades, μg m^{-3}) of SO_4^{2-} and NO_3^- averaged over 70–105°E in June-August of 2005, together with the wind vectors obtained from the European Centre for Medium-Range Weather Forecasts (ECMWF) ERA-Interim Reanalysis data. The black line is the tropopause simulated by the GEOS-Chem model.
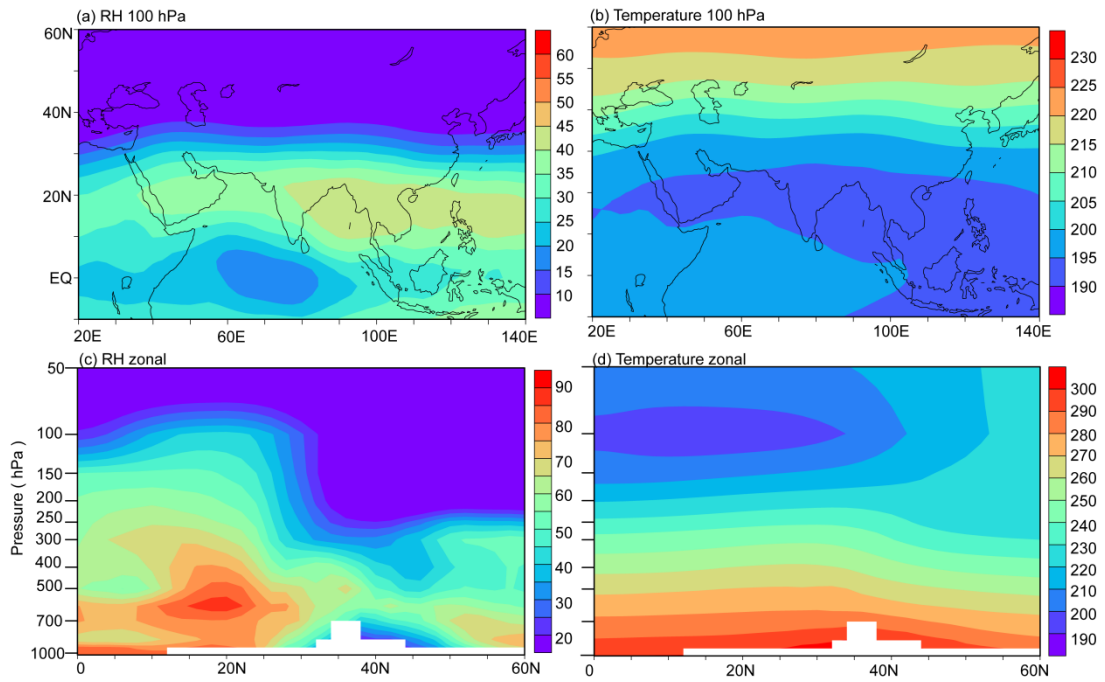
Figure. 12. (a)-(b) Distributions of RH (%) and temperature (K) at 100 hPa. (c)-(d) The latitude-altitude cross sections of RH (%) and temperature (K) averaged over 70−105°E. RH and temperature are from the GEOS5 assimilated meteorological fields, and all the values are the averages over June-August of year 2005.
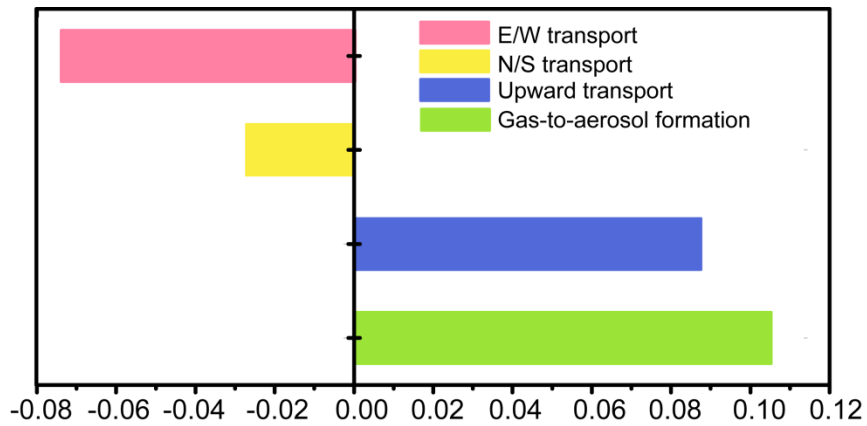
Figure. 13. Mass budget for nitrate aerosol within the selected box of (70–105°E, 10–40°N, 8–16 km). E/W transport indicates net mass flux through the east and west lateral boundaries, N/S transport indicates net mass flux through the north and south lateral boundaries, and upward transport is the net mass flux through the top and bottom sides of the box. The mass flux is positive if it increases nitrate mass within the box. Unit of fluxes is Tg season^{-1}. All the values are the averages over June-August of 2005.